Effect of frequency, R-ratio and test specimen configuration on fatigue crack growth in PE pipe materials

Diploma Thesis
by
Hannes Stadler

Institute for Materials Science and Testing of Plastics
of the University of Leoben
and
Polymer Competence Center Leoben GmbH

Supervisor: Dipl.-Ing. Dr. Werner Balika

Dipl.-Ing. Dr. Gerald Pinter

Assessor: o. Univ.-Prof. Dipl.-Ing. Dr. Reinhold W. Lang

Leoben, November 2006

Acknowledgements

I would like to thank o. Univ.-Prof. Dipl.-Ing. Dr. Reinhold W. Lang, of the Institute for Materials Science and Testing of Plastics of the University of Leoben and the Polymer Competence Center Leoben GmbH, for enabling this diploma thesis, and for his expertise and the correction of my work.

My best thanks go to my supervisors, Dipl.-Ing. Dr. Werner Balika and to Dipl.-Ing. Dr. Gerald Pinter who have followed every aspect of this thesis from the very first day and showed the highest willingness towards me at every moment. During the last few months they have always listened to my questions and problems and have given me helpful suggestions on the completion of this work.

I would like to thank Ms. Kay Fisher, for the proofreading of the final version of this diploma thesis, and all the staff of the PCCL and the Institute for Materials Science and Testing of Plastics of the University of Leoben for their constant support in resolving all the difficulties, large and small, that I have encountered during my work at the Institute.

Finally, I want to thank Andrea and my parents for their patience with me during this last year and before.

Table of Contents

Abstract

In the work presented here, fatigue crack growth (FCG) experiments were performed on three commercial polyethylene (PE-HD) pipe grades with a bimodal molecular weight distribution. In order to investigate the influence of different specimen types on FCG results, tests were conducted using compact type (CT) specimens and cracked round bar (CRB) specimens. One objective of this investigation was the design and implementation of grips for CRB testing and the optimisation of the loading procedure for FCG testing. The effects of R-ratio and frequency on FCG behaviour were also studied.

A discontinuous crack growth mechanism was characteristic for all materials investigated, which was well visible by typical arrest lines on the fracture surfaces of CT and CRB specimens. In CT specimens, crack growth inside the specimen (under plane strain conditions) was higher than on the outside, which can be noted from the semi-elliptical shape of the front-line of the crack. By comparing the materials it turned out that the molecular weight should be the most important parameter for the increase in FCG resistance.

The main reason for selecting CRB specimens was the well-defined plane strain condition in the ligament. Quasi-brittle cracks could be initiated, but it was very difficult to achieve symmetrically growing cracks. On the basis of the results gained so far, testing time was clearly reduced using CRB rather than CT specimens, which could be of particular interest when the goal is the ranking of materials. The effects of frequency may be considered significant in the low crack growth region. It was found out that with increasing test frequency there was a noticeable increase in crack growth resistance in CT specimens in the low crack-growth regime, while in CRB specimens no differences could be found because of the large scatter band. For all investigated frequencies, a temperature increase resulting from hysteretic heating was measured at the crack tip in CT specimens.

FCG rates showed a great dependence on R-ratio in terms of the stress intensity factor range. There may be a tendency for higher crack growth rates at higher R-ratios as a result of more creep crack extension associated with the higher maximum and mean stress intensity factor levels.

Kurzfassung

In der gegenständlichen Arbeit wurden Ermüdungsrissversuche an drei Polyethylen-Rohrwerkstoffen mit hoher Dichte (PE-HD) durchgeführt. Es handelt sich dabei um Typen mit einer bimodalen Molekulargewichtsverteilung. Um den Einfluss von verschiedenen Prüfkörperkonfigurationen zu untersuchen wurden zusätzlich zum "Compact Type (CT)"-Prüfkörper auch "Cracked Rounded Bar (CRB)"-Prüfkörper verwendet. Eine Zielsetzung dieser Arbeit war die Entwicklung einer Einspannvorrichtung für das Testen von CRB-Prüfkörper und die Optimierung der Belastungsvorgänge für Ermüdungsrissversuche. Zusätzlich wurden der Einfluss des R-Verhältnisses und der Frequenz untersucht.

Charakteristisch für alle untersuchten Materialien war ein diskontinuierliches Risswachstum, welches durch typische Haltelinien gut auf den Bruchoberflächen der CT- und CRB-Prüfkörper sichtbar war. Im Inneren des Prüfkörpers, also im Bereich ebener Dehnung war das Risswachstum höher als an der Aussenseite, was auch an einer nahezu halb-elliptischen Form der Rissfront erkennbar war. Beim Vergleich der Materialien stellte sich heraus, das ein zunehmender Widerstand gegen Ermüdungsrisswachstum hauptsächlich durch das Molekulargewicht bestimmt wird.

Der Hauptgrund für die Verwendung von CRB-Prüfkörpern ist die Gegebenheit eines eindeutig ebenes Dehnungzustand im Restquerschnitt. Es war möglich quasi-spröde Risse zu initiieren, aber schwer symmetrisch wachsende Risse zu erhalten. Auf der Basis bisher erhaltener Messergebnisse wurde festgestellt das sich die Prüfzeiten bei der Verwendung von CRB- anstatt CT-Prüfkörpern deutlich reduzieren. Das kann speziell dann interessant sein, wenn ein Material-Ranking gewünscht ist.

Der Einfluss der Frequenz ist besonders bedeutend im Bereich des langsamen Risswachstums. Bei CT-Prüfköpern wurde mit zunehmender Testfrequenz ein deutlicher Anstieg des Widerstands gegen Risswachstums festgestellt. Währendessen konnten bei CRB-Prüfkörpern aufgrund der großen Streuung der Ergebnisse keine Unterschiede gefunden werden. Bei allen untersuchten Frequenzen wurde an der Rissspitze von CT-Prüfkörpern eine

Temperaturzunahme, bedingt durch hysteretische Erwärmung gemessen. Einen großen Einfluß auf das Ermüdungsrisswachstum zeigt das R-Verhältnis. Bei höheren R-Verhältnissen zeigt sich tendenziell eine Zunahme der Risswachstumsraten als Resultat höherer Niveaus von Maximal- und Mittelspannungsintensitätfaktor.

1   Introduction and Objectives

Among all thermoplastic materials processed in the pipe industry, polyethylene (PE) and polyvinyl chloride (PVC) are the two most important materials on the market, especially high density polyethylene (PE-HD) and unplasticized polyvinyl chloride (PVC-U). In terms of areas of use, the percentages of PE-HD was 20 % in pipe applications in Western Europe, while for PVC-U 24% was found, [Beer et al., 2005; Ertl et al., 2004; Glenz, 2004; Hohenadel et al., 2005]. While global PE-HD capacity was approximately 33 million tons (33 m t) in 2004, global PE-HD sales increased by 4.3 % to some 25.5 m t between 2000 and 2003 [Beer et al., 2005; Glenz, 2004]. In comparison to PE-HD, global PVC capacity was a little higher (35 m t). Global PVC consumption ran at some 29 m t in 2004 and has grown by approximately 4 % since 2000 [Ertl et al., 2004; Hohenadel et al., 2005]. Average growth rates of 6 % for PE-HD and 3.5 % for PVC are expected worldwide over the next few years. Today it is well known that an understanding of the creep crack growth (CCG) phenomenon is one of the most important factors in the evaluation of the long-term performance of thermoplastic plastic pipes. It is also well established that quasi-brittle failure consisting of crack initiation and crack propagation can be realized in principle under laboratory conditions by various mechanical approaches. In regard to a reduction of testing time, the main principle of all concepts is to tighten significant test parameters like temperature, applied stress, environmental conditions (surfactants) and loading condition [Fleissner, 1987; Hertzberg and Manson, 1989; Lang et al., 2000; Laurent, 2001; Song et al., 1998; Williams, 1987]. Due to the complexity of the failure and aging mechanisms which all strongly depend on time and temperature, there are still some limitations to the applicability of these test data for a flawless lifetime prediction of thermoplastic plastic pipes under real service conditions [Dörner and Lang, 1997; Lang et al., 2000; Lang et al., 1997; Pinter and Lang, 2004; Song et al., 1998].

Despite the basic difference in loading conditions, some research groups favor fatigue test approaches in evaluating new pipe grades and in evaluating the long-term performance under constant loading conditions for the following reasons: Firstly, fatigue loading principally leads to accelerated crack growth; secondly,

similar characteristics have been found in creep crack growth and fatigue crack growth (FCG) in various PE and PVC-U materials [Balika et al., 2004; Hu et al., 2003; Kadota et al., 1993; Kasakevich et al., 1990; Reynolds and Lawrence, 1991]. Although many research groups over the last 15 years or so have concentrated their efforts on studying the correlation between the kinetics of crack growth under static and cyclic loads [Chudnovsky et al., 1995; Parsons et al., 1999, 2000b; Pinter et al., 2002a; van der Grinten and Wichers Schreur, 1996; Zhou and Brown, 1992] there are still many open issues to clear up, which will be discussed in more detail in chapter 2. In addition to experimental attempts, simulation tools are today commonly used in materials science. With regard to the further development of models that describe crack growth characteristics in terms of kinetic data, such as the crack layer model by Chudnovsky [Chudnovsky, 1984; Chudnovsky et al., 1995], more experimental data are needed.

The main objective of this diploma thesis is to characterize the fatigue crack growth behavior of various PE-HD pipe grade materials (PE 100 types) using a method based on a linear elastic fracture mechanics (LEFM) approach. As a basic step for a comparison of FCG and CCG data, the effects of mean stress (i.e., R-ratio = minimum load/maximum load), frequency, and specimen configuration were systematically investigated at room temperature.

2 General Background

2.1 Polyethylene pipe grade materials

Historically, the classification of PE resins has developed in conjunction with the discovery of new catalysts for polyethylene polymerization as well as new polymerization processes and applications and is based on the resin density and its melt flow rate (MFR). From the start of the industrial production of polyethylene resins in the 1950s, both parameters could easily be measured in a commercial environment with minimum instrumentation. Table 2.1 gives an overview of PE materials in terms of the historical (or commercial) classification [Kissin, 1996]. Although this method provides a simple means for a basic differentiation of PE resins, it is interesting to note that discrepancies were found in the literature while comparing the classification ranges of the various polyethylene types. Comparing three different sources [Domininghaus, 1997; Kissin, 1996; Lederer and Forster, 1984], it can be concluded that the discrepancies are ascertainable, but not really significant (see Table 2.2). The big disadvantage of this classification in its present form is that it cannot easily describe some important distinctions between the structure and properties of various resin brands.

Table 2.1: Historical or commercial classification of polyethylenes [Kissin, 1996].

Designation	Acronym	Density [g/cm^3]
High density polyethylene	PE-HD	$\geq$ 0.941
Ultrahigh molecular weight polyethylene	PE-UHMW	0.935 - 0.930
Medium density polyethylene	PE-MD	0.926 - 0.940
Linear low density polyethylene[a]	PE-LLD	0.915 - 0.925
Low density polyethylene	PE-LD	0.910 - 0.940
Very low density polyethylene[b]	PE-VLD	0.880 - 0.915

[a] Linear polymer with molecular weight of over 3 x 10^6.
[b] Produced in high pressure processes.

Table 2.2: Comparison of historical classification data from three different sources.

Designation	Density [g/cm^3]		
	Lederer, 1984	**Kissin, 1996**	**Domininghaus, 1997**
PE-HD	0.940 - 0.970	0.940 - 0.970	≥0.941
PE-MD	0.925 - 0.940	0.930 - 0.940	0.926 - 0.940
PE-LD	0.910 - 0.935	0.915 - 0.935	0.910 - 0.940
PE-LLD	0.910 - 0.940	0.900 - 0.930	0.915 - 0.925

Today, a newer classification is commonly used for PE pipe grade materials, based on the minimum required strength (MRS). Each class is denoted by a number that is obtained by multiplying the MRS, expressed in MPa, by 10. The MRS value must be used when designing long-term loaded PE pipes operating at a temperature of +20 °C for at least 50 years.

To obtain the MRS value, multiple internal pressure tests are performed at different pressure levels and temperatures. A typical creep-rupture curve showing the different stages and the corresponding failure modes is given in Fig. 2.1. Three stages can be seen. The first stage, at high stress levels, corresponds to ductile failure, which often appears with the bulging of the pipe cross-section. During the second stage, at lower stresses, the pipe fails in a brittle or quasi-brittle mode after the initiation and propagation of a crack, usually from the inner surface. At very low applied stress levels, failure is due to chemical aging (thermal oxidation) with a substantial degradation of the polymer (3rd stage).

By dividing the MRS value by a safety factor of 1.25 (which is also called the design factor C, according to ISO 12162), the design hoop tensile stress can be calculated:

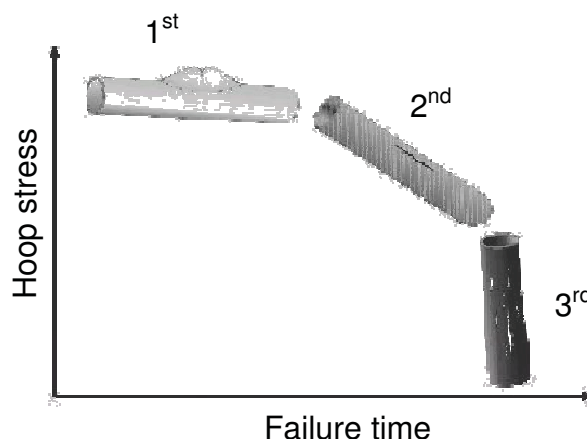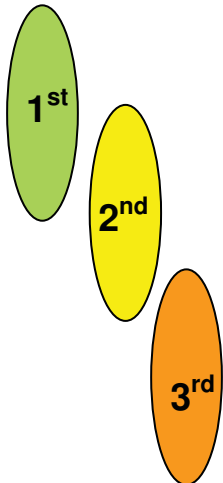$$\sigma_D = \frac{MRS}{C} \tag{2.1}$$

Fig. 2.1: Creep-rupture curve of plastic pipes (at high temperatures) [Fanesi, 2003].

To date, three generations of PE have entered the pipe market. Due to their MRS values of 6.3 MPa and 8 MPa, the first and second generations were classified as PE 63 and PE 80. It is interesting to note that PE 32 and PE 40 materials are casually included with the first generation resins. Since the 1990s, a third generation of high density polyethylene resin has been developed, the main characteristic of which is a bimodal molecular weight distribution (MWD) [Hubert et al., 2001; Janson, 1999]. The introduction of bimodal copolymers made it possible to reach an MRS of 10 MPa, thus opening the market to PE 100 materials. While PE 80 grades are primarily based on the Phillips chromium catalysts, the PE 100 resins are based on Ziegler-Natta catalysts, which lack the melt elasticity of the earlier grades [DesLauriers et al., 2005]. It should be noted that bimodal PE 80 materials also exist, since bimodality deals with molecular structure characteristics and not directly with the internal pressure strength like the MRS value. The next step in the development of PE pipe materials is expected to result in a PE 125 type, cor-responding to an MRS value of 12.5 MPa. All information given above is summarized in Table 2.3.

Bimodal PE differs significantly from the two older, unimodal, generations in its molecular architecture. In unimodal copolymers, due to an intrinsic feature of the polymerization process, short chain branching content (SCB) is located mainly on the medium-low molecular weight chains. "Bimodal" signifies that the copolymer has two different types of molecular chains; almost perfect linear chains

Table 2.3:   Classification of PE pipe materials based on the MRS value accord-
ing to [Hubert et al., 2001; Janson, 1999].

Generation	Designation	Classification number	MRS [MPa]	σ_D [1] [MPa]
1st / 2nd / 3rd	PE 32	32	3.2	2.5
	PE 40	40	4.0	3.2
	PE 63	63	6.3	5.0
	PE 80	80	8.0	6.3
	PE 100	100	10.0	8.3
	PE 125	125	12.5	10

1) C=1.25 in water

characterize the low molecular weights, while the side branches, whose length de-
pends on the choice of the comonomer, are preferentially located on the longer
macromolecules. So high impact strength, stress crack resistance, stiffness, ten-
sile strength and good processability are combined, and materials with outstanding
properties are achieved.

The different techniques that have been proposed to produce different polymers
with bimodal MWD can be summarized [Bäckman and Lind, 2001; Ha et al., 1998;
Kim and Wang, 1994; Li and Wang, 2003] as either:

1. Stepwise polymerization in a tandem reactor (e.g. two-stage process);

2. Polymerization using mixtures of different catalysts;

3. (Sudden) variation of reaction/operation conditions in a single reactor during
    polymerization (especially the concentration of chain transfer agent, tem-
    perature, monomer concentration and hydrogen pressure), or;

4. Physical blending of polyethylene resins with different molecular weights.
    This method has been reported in several instances.

Up to now, the first technique has been the prevailing industrial method used to produce bimodal polyethylene in two or more cascaded reactors [Andersson et al, 2004]. Under extremely different reaction conditions in each step of the polymerization process, and using an advanced Ziegler-Natta or single site type catalyst, a polyethylene blend is formed. The two-stage processes bring substantial flexibility in tailoring polymer structure and properties [Krumme et al., 2003] but according to some authors this method is expensive, cumbersome and time-consuming [Li and Wang, 2003].

The idea behind the selective combination of catalysts is to combine, within each catalyst particle, two catalyst components that operate under identical conditions but produce polymers with radically different molecular weights. This method is assumed to be an elegant and cost-efficient way to produce polyolefins with controlled microstructures, but several practical problems must be addressed before this approach is implemented industrially [Soares and Kim, 1999].

Non-steady-state polymerization in a single reactor with sudden variation of reaction/operation conditions is effective for laboratory-scale reactors, but it is unlikely to be applied to the production of commodity polyolefins [Soares and Kim, 1999].

Current developments have shown that multimodal (two or more) molecular weight resins can be made using a single catalyst in a single reactor. This catalyst contains two sets of sites which selectively respond to reactor conditions to produce tailored, multimodal weight resins [DesLauriers et al., 2005].

2.2 Testing methods for slow crack growth characterization in PE pipe grade materials

Today it is well known that an understanding of the quasi-brittle failure phenomenon is one of the most important factors in the evaluation of the long-term behavior of thermoplastics pipes. It is generally acknowledged that the origin of this phenomenon is the formation, growth and failure of plastic zones at places of stress concentration. Although, in the literature, the resistance against crack propagation is predominantly attributed to the phenomenon of chain-disentanglement, there are enough indications for chain fracture playing an important role in this context

[Hubert et al., 2001; Kausch, 1986; Kramer and Berger, 1990; Ramsteiner, 2004]. Especially, newer investigations by Lang and Pinter [Lang, 1997; Pinter, 1999; Pinter and Lang, 2003, 2004] on polyethylene have strengthened the hypothesis that local crack-tip aging processes affect the kinetics of crack propagation.

An overview of the most important parameters that control the phenomenon of slow crack growth (SCG) is shown in Fig. 2.2 and Fig. 2.3. While the polymer structure (molecular mass and molecular mass distribution, branching) and morphology (crystalline and/or amorphous zones, lamellas) play an important role, the influences of processing parameters, fillers and reinforcement materials, additives, stabilizers and testing conditions must also be considered in discussing the failure behavior of polymeric materials [Brown and Lu, 1995; Egan and Delatycki, 1995; Karger-Kocsis, 1995; Nezbedova et al., 2001; Pinter, 1999; Pinter et al., 2000].

Since the 1950s, a large number of tests have been proposed to verify the SCG phenomenon as realistically as possible in the laboratory. Internal pressure tests
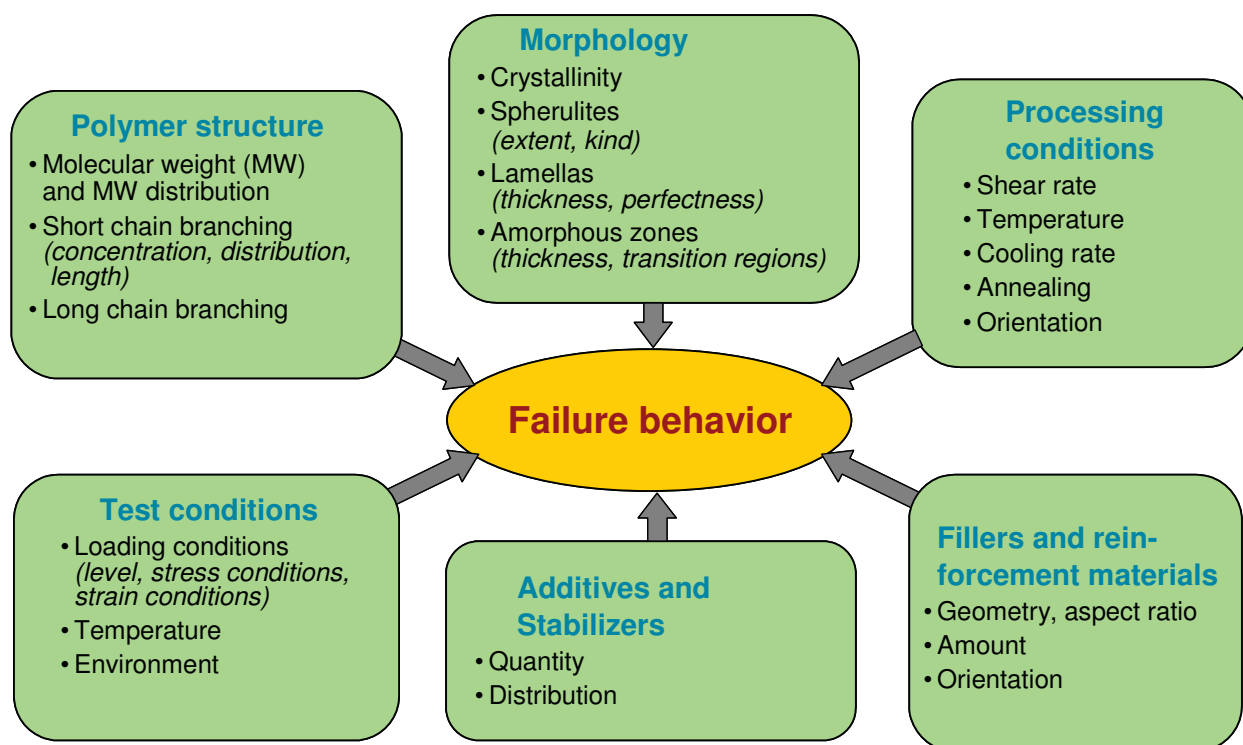

Fig. 2.2: Factors influencing failure behavior, after [Egan and Delatycki, 1995; Karger-Kocsis, 1995].
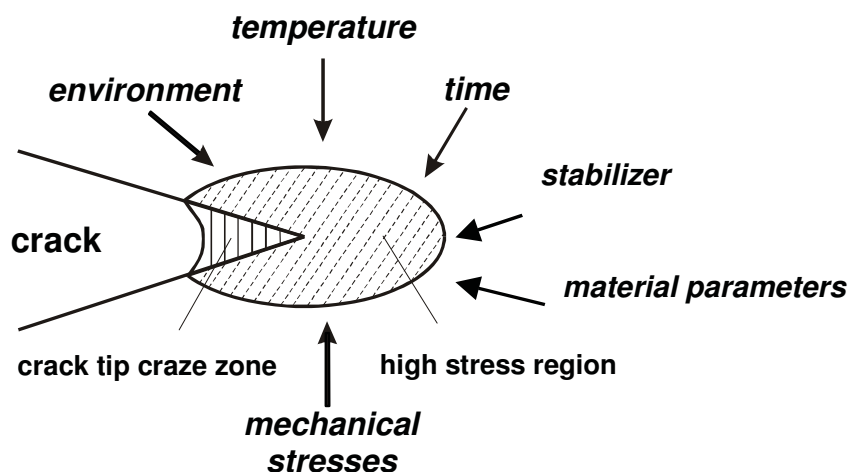
Fig. 2.3: Factors influencing SCG.

on pipe specimens are the traditional way to determine the long-term properties of PE pipes. Unfortunately this method is expensive and time-consuming. The development of third-generation resins in particular has led to the tests exceeding practicable time frames. Consequently, due to the requirement for quicker test methods, several fracture mechanics methods have been introduced during the past 15 years to characterize SCG in PE pipe materials and to obtain information on the long-term behavior within a reasonable time frame.

Presently, the internal pressure test, the cone test, the notched pipe test, the Pennsylvania notch tensile test (PENT-test), the full notch creep test (FNCT), and the accelerated relaxation and end load test (AREL-test) are regulated by standards. At the moment, another two test methods (point loading test, notched ring test) are under discussion for standardization [Dragaun and Kratochvilla, 2004].

Standardized test methods for SCG:

The **internal pressure test** *(ISO 1167 and EN 921)* specifies a method to establish the resistance to constant internal pressure at constant temperature. In order to achieve the desired internal pressure, test samples cut from pipes are filled with water. The test is carried out in a controlled environment, which can be either water or a different liquid, or air. The time to failure is then recorded. The ISO standard requires a minimum testing time of 100 h at 20 °C and 12.4 MPa for PE 100, 9 MPa for PE 80 materials, while at 80 °C the minimum becomes 165 h at 5.5 MPa for PE 100, 4.6 MPa for PE 80.

The **cone test** *(ISO 13480:1997-09-15)* is also widely used throughout the industry*.* A constant stress is created over the pipe cross-section by pressing a conus into the pipe. A notch is cut at one end and the specimen is tested at 80ºC in a surfactant solution (see Fig. 2.4). The crack growth after initiation is measured and the largest value for crack growth is determined.
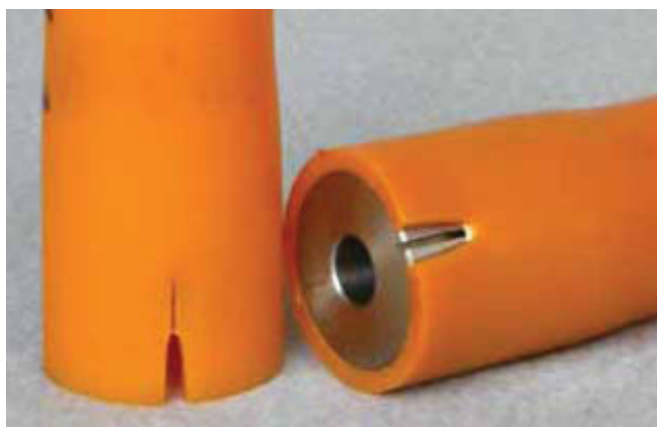

Fig. 2.4: Experimental set-up for the cone test.

The **notched pipe test (NPT)** (*ISO 13479)* is used to evaluate the stress crack resistance of pipes, since it simulates slow crack growth [Beech et al, 2005]. Samples of free length are cut from a pipe and four equally spaced axial V-notches are machined in the outer surface around the pipe circumference (see Fig 2.5). This creates a stress concentration, which promotes crack growth and simulates the effect of surface damage that might occur during installation. The test is performed at 80 ºC at well-defined pressure levels and the time to failure is
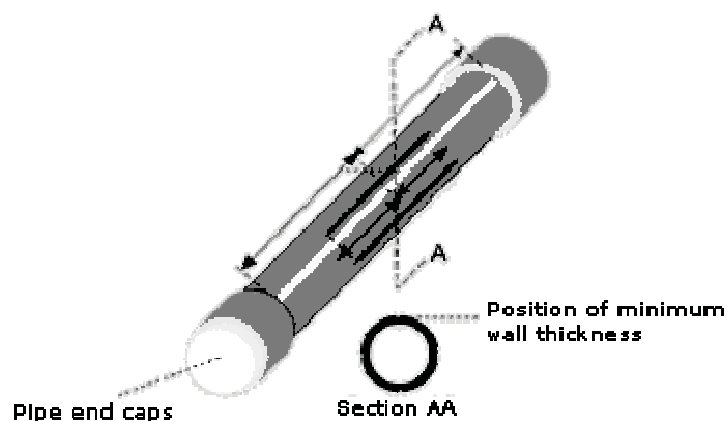

Fig. 2.5: Specimen configuration for the notched pipe test.

recorded. The time to failure becomes one of the factors that are taken into account to classify the polymer as belonging to a particular class: for example for both PE 80 and PE 100 the standard requires a testing time of at least 165 h at 80 °C under a nominal plane pipe hydrostatic stress level of 4.0 MPa for PE 80 and 4.6 MPa for PE 100 materials.

The **Pennsylvania notch tensile test (PENT)** *(ISO/FDIS 16241:2003-12)* was developed by Brown at the University of Pennsylvania to simulate the fracture process that occurs during long-term failure of polyethylene pipes. A specimen machined from compression-molded plaques is notched on three edges and exposed to a constant load (a tensile stress of 2.4 MPa) in air at 80 ºC. The temperature of 80 ºC is based on the consideration that the failure mechanism under these conditions will be representative of that at lower operating temperatures. This test determines resistance to SCG by measuring the total time to failure [Brown et al. 2005].

The **full notch creep test (FNCT)** was initially used by [Nishio et al] and is especially popular in Europe (Germany) for the characterization of SCG in PE pipe materials [Beech and Clutton, 2004; Beech et al., 1997; Fleissner, 1998; Grosse-Boes and Kloth, 2004; Haager et al., 2004; Kratochvilla et al., 2005]. The test is currently standardized in *ISO 16770.3* and *EN 12814-3* in order to establish uniform test conditions enabling the use of the FNCT for material specifications. The method can be described as a tensile constant load test, performed at elevated temperatures on notched specimens (see Fig 2.6) designed to favor SCG. Often a surface-active environment is used to accelerate the test. The test has been described relatively often and a multitude of test conditions have been mentioned by different authors, making it difficult to compare the results. Currently, strong efforts are being made to standardize the test parameters, but no generally accepted test conditions have yet been established, although the establishment of material specifications is being increasingly discussed. Moreover, Hessel has stated in several published articles that FNCT can be used to ensure a lifetime of 50 years for PE pipes [Hessel, 2001]. The FNCT test has gained more interest in Europe than the PENT test, because it is able to reduce failure times even using the synergic effect of a surfactant detergent.
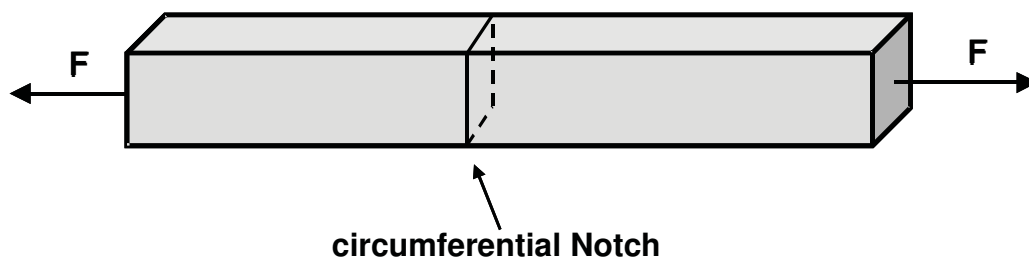
circumferential Notch

Fig. 2.6: Specimen configuration for FNCT.

The **accelerated relaxation and end load (AREL) test** according to *ISO/CD 19899* was developed for the determination of the "stress crack failure" in a piping system (see Fig. 2.7). A section of a pipe is exposed to a constant load (a tensile stress of 3 MPa) in air or water at 80°C for 500h. Afterwards the system is released and tested for impermeability with compressed air at 25mbar.
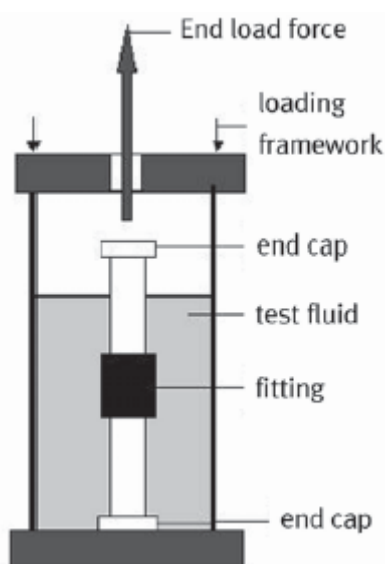

Fig. 2.7: Experimental set-up for the AREL test.

Non-standardized test methods for SCG:

The aim of the **point loading test** *(DVGW VP 641)* is to simulate the influences of non-conventional pipe laying without a sandbed in order to gain a lifetime prediction for PE pipes, and is based on the research work of Hessel [Hessel, 2001]. Pressurized pipes are loaded using an external point load at a temperature of 80 ºC and a surfactant detergent to accelerate the test. The external point load is applied before starting the internal pressure test. The required surface elongation at the inner pipe wall (i.e. the above yield elongation) is produced by the displace-

ment of a tool along the radius of the pipe. For a hoop stress of 4 MPa, a minimum lifetime of 8760 h is required.

The **notched ring test** (NRT) was developed by the University of Hannam, Korea, and firstly presented in September 2004 at the *ISO/TC138* plenary session in Nice. The test sample cut from a pipe is notched inside and exposed with a linear distributed load as shown in Fig. 2.7, which is very similar to common 3-point-bending tests. The NRT is performed at 80 ºC in air or water without using a surfactant detergent. The deformation due to the applied load is measured. Compared to the notched pipe test, testing time is expected to drop dramatically.

Fig. 2.8: Experimental set-up for the NRT.

Another **test system, based on the linear elastic fracture mechanics approach** is shown in Fig. 2.9. While other test systems only allows the determination of total failure times, it is possible to study crack growth kinetics and specimen creep under static load. The experimental data is employed for lifetime prediction using a simple fracture mechanical calculation model [Lang et al., 1997; Stern, 1995]. Test can be performed at varying temperatures and in different environments.

The development and implementation of all of the above test methods was focused on the main objective of having a test procedure that allows the prediction of a minimum service life of currently 50 (to possibly 100) years. While many polymer physics aspects are included in these concepts, there are some open
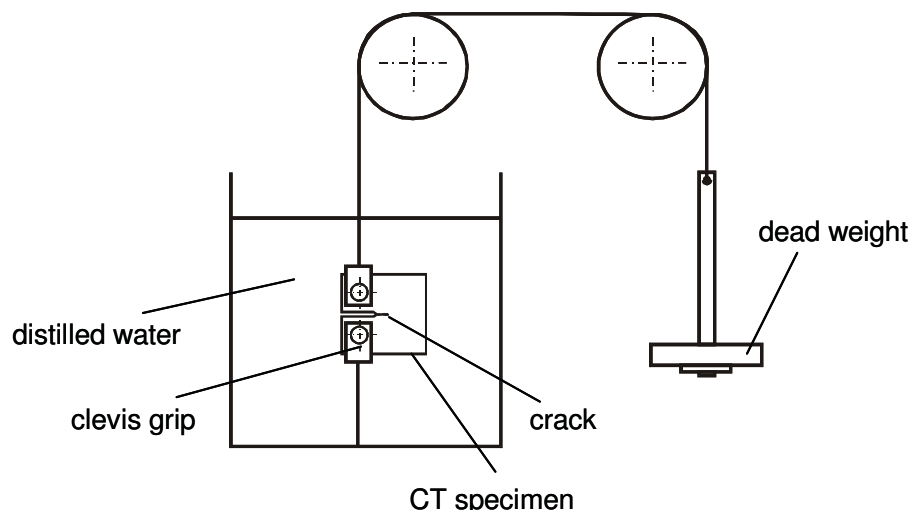
Fig. 2.9: Schematic representation of the test apparatus for creep crack growth
tests under static loads.

issues, especially with regard to the transferability of the experimental data to the
long-term performance of thermoplastics pipes under service conditions. Two main
issues are discussed in the recent literature: firstly, the extrapolation to service life
at the temperature of use is often based on data determined at elevated
temperatures, where problems are assumed due to possibly complex aging
mechanisms at higher temperatures [Lang et al., 1997; Song et al., 1998];
secondly, the detailed effects of surfactant detergents on SCG are not clear. The
question of whether the aggressive environmental conditions lead to changes in
the mechanisms of failure and therefore do not reflect real field conditions, is dis-
cussed quite controversially in the literature [Hessel and Maurer, 1994; Scholten et
al., 2001; Scholten et al., 1998].

2.3 Fatigue crack growth in PE pipe materials

The idea of applying fatigue loading in evaluating new pipe material grades,
especially in terms of performance ranking, and moreover in evaluating the long-
term performance under constant loading conditions, is not new. Despite the basic
differences in loading conditions, investigations on polyethylene (PE) have shown
that there are similar characteristics in creep crack growth and fatigue crack
growth [Parsons et al., 1999, 2000b; Pinter et al., 2002c; van der Grinten and
Wichers Schreur, 1996]. While fatigue loading principally leads to accelerated
crack growth, there are some issues that will be discussed in detail below.

2.3.1 Effect of frequency

Many investigations of PE materials have shown that FCG rates decrease with in-creasing frequency at constant values of stress intensity factor range [van der Grinten and Wichers Schreur, 1996]. This is also true of several other polymers such as poly(methyl methacrylate) (PMMA), polystyrene (PS), polyvinyl chloride (PVC) and polyamide (PA) [Hertzberg and Manson, 1980; Lang, 1984], while other polymers such as polycarbonate (PC) and polysulfone (PSU) show no apparent sensitivity of FCG rates to test frequency. Hertzberg and Manson [1980] investi-gated the effect of frequency on the FCG behavior of different amorphous poly-mers using the frequency sensitivity factor (FSF). A strong connection has been established between gross mechanical properties (FCG response) and the fine-scale viscoelastic response of polymeric solids. It has been shown that the FSF for a given polymer depends strongly on the frequency of movement of the main chain segments responsible for generating the principle secondary transition peak (β-peak). The greatest FCG frequency sensitivity occurs when the test frequency is close to the frequency of the β-process. Conversely, the β-frequency is far above the test range for insensitive materials. In addition, the maximum sensitivity of FCG to frequency in engineering plastics occurs at a particular temperature that is unique to the material and related to a β-transition. At temperatures sufficiently above or below the region of the β-transition, crack growth rates are essentially frequency independent.

Lang [1984] has pointed out the complexity of interactions, where the local strain rate at the crack tip, the loading rate, the load-time integrated area per cycle and hysteretic heating (in regions near to the crack tip as well as far away from the crack tip) play an important role. Based on his investigations, some facts indicate that the physical interpretation of the FSF model may be incorrect. It has been speculated that blunting of the crack tip due to a temperature gradient across the process zone in front of the crack might also contribute to the enhancement in FCG resistance at higher test frequencies [Rimnac, 1983]. Investigations of the cyclic deformation within the process zone may provide a better mechanistic ex-planation to rationalize FCG frequency sensitivity in polymeric materials.

2.3.2 Effect of the R-ratio

The stress ratio (R-ratio) is defined as the ratio between the minimum and the maximum applied loads, which is equal to the ratio between the minimum and the maximum stress intensity factors (equation 2.2). Many studies have been conducted on different PE materials to evaluate the effect of the R-ratio (i.e. mean stress) on the rate of crack propagation at different levels of stress intensity factor range, ΔK [Brown and Lu, 1994; Bucknall and Dumpleton, 1985; Haager et al., 2005a; Pinter et al., 2002b; van der Grinten and Wichers Schreur, 1996]. In terms of ΔK, two different effects were detected in these investigations. On the one hand, FCG rates increased with increasing R-ratio. On the other hand, no apparent sensitivity of FCG rates to R-ratio was observed. Apparently, mean stress effects on the fatigue response of polymeric solids are dependent on two conflicting processes [Hertzberg and Manson, 1980]: (1) Assuming a constant stress intensity factor range, there may be a tendency towards higher FCG rates as a result of increased creep crack extension associated with higher K_{max} levels and also because K_{max} approaches the critical limiting value for the material (i.e., K_c). (2) Alternately, there may be a strain-induced modification of the polymer substructure, thereby making the fatigue process more difficult and resulting in lower fatigue crack growth rates.

$$R = \frac{F_{min}}{F_{max}} = \frac{K_{min}}{K_{max}} \tag{2.2}$$

Due to the different effects of the R-ratio on FCG rates in polyethylenes, there are different opinions about the parameters that control fatigue crack propagation in PE materials. While some authors declare the stress intensity factor range to be the most important factor, the research group of Baer and Hiltner [Parsons et al., 1999, 2000b] in particular has proposed that the FCG rate is a function of the maximum stress intensity factor K_{max} and mean stress intensity factor K_{mean}.

2.3.3 Correlations between CCG and FCG kinetics

There is a great agreement in the literature that the effects of frequency and the R-ratio on FCG behaviour are the result of a combination of fatigue and creep components. Although a simple superposition model involving pure fatigue and creep

components (equation 2.3) seems to be both unreasonable and oversimplistic [Skibo, 1977], the explanation of many authors is based on this model [Clark et al., 1990; Miannay, 2001; Parsons et al., 2000a; Pinter et al., 2002b; Saxena, 1998; van der Grinten and Wichers Schreur, 1996]. It is interesting that no comments are given on the possible interactions between the two components. Parsons et al. [2000b] concluded that a fatigue test might behave like a creep test at a low enough frequency, which means that fracture is completely controlled by creep processes even though the load is cyclical. This is in good correlation with the interpretation in [Pinter et al., 2002b; van der Grinten and Wichers Schreur, 1996], where the influence of the creep component increases with increasing test temperature. In addition, it is considered that the fatigue component of loading depends only on the strain rate, assuming that hysteretic heating is minimized using test frequencies of or below 1 Hz. Similar to the well-known Paris-Erdogan relationship (equation 2.4), the research group of Baer and Hiltner [Parsons et al., 2000a] has proposed that in this case the crack growth rate in fatigue can be characterized by a contribution from the creep process, multiplied by a fatigue acceleration factor, β, that is a function of strain rate only (equation 2.5).

$$\left(\frac{da}{dN}\right)_{total} = \left(\frac{da}{dN}\right)_{fatigue} + \frac{1}{f}\left(\frac{da}{dt}\right)_{creep} \tag{2.3}$$

$$\frac{da}{dN} = A \cdot \Delta K^m \tag{2.4}$$

$$\frac{da}{dt} = B\left\langle K_I^4(t)\right\rangle_T \beta(\dot{\varepsilon}) \tag{2.5}$$

where a is the crack length, N is the number of cycles, f is the frequency, ΔK is the stress intensity factor range, A and m are constants which depend on the material as well as on test variables such as temperature and environment, K_I is the stress intensity factor, T is the fatigue cycle period and $\dot{\varepsilon}$ is the strain rate.

2.3.4 Effect of the specimen configuration

In different fatigue tests for PE resins there is a great variation in the specimen configuration. While some fatigue tests are conducted on sections of the pipe

[Lawrence et al., 1998; Reynolds and Lawrence, 1991, 1993; Shah et al., 1998a, 1998b] and on specimens cut directly from the pipe [Nishimura et al., 1993; Shah et al., 1998c; Shah et al., 1998a, 1998b], it has become quite common to cut specimens from compression-molded plaques, especially when the development and/or ranking of materials are the major objectives. Among all the specimens used in fatigue tests based on fracture mechanics concepts, the compact type (CT) specimen has become the most important one, which is reflected by the many examples in the literature of the last 30 years [Kuske and Bastian, 2004; Parsons et al., 2000b, 2001; Shah et al., 1998a, 1998b]. Other fatigue experiments have been performed, for instance, using single edge notched tensile (SENT) specimens, center cracked tension (CCT) specimens and the wedge open loading (WOL) specimens [Bucknall and Dumpleton, 1985; Strebel and Moet, 1995; van der Grinten and Wichers Schreur, 1996; Zhou and Brown, 1992]. It should be mentioned that the CT and SENT specimens are the standardized specimen types in ISO 15 850, where the determination of the fatigue crack propagation in PE materials is based on a linear elastic fracture mechanics (LEFM) approach. In the last few years, various types of notched bars with round or square cross-sections have gained more and more importance in the testing of PE under cyclic loading conditions [Plummer et al., 2001, 2003; Zhou and Brown, 1989]. In comparison to CT and other specimens, preference is especially given to notched round bars for the following complementary reasons: (1) the geometry is very simple and can be obtained with a single machining technique, (2) the initial notch is applied very smoothly which is favorable for optimum crack initiation, (3) the crack profile can be monitored throughout the whole test without any problem of concavity which would hide the actual crack tip, and (4) the plane strain condition is relatively well-defined in the ligament [Favier et al., 2002].

3 Methodology and Experimental

3.1 Materials and specimen preparation

All investigations reported in this work were performed on three commercial PE-HD pipe grades (DOW Chemical, Switzerland and USA). The three resins have a bimodal molecular weight distribution and, having an MRS = 10 MPa, are classified as PE 100 materials. In this report they have been named PE100-1, PE100-2 and PE100-3. PE100-1 is a black, carbon filled type, PE100-2 and PE100-3 are natural ones. An overview of the investigated PE 100 materials is given in Table 3.1. The main characteristic mechanical and molecular properties are summarized in Table 3.2. and Table 3.3.

Table 3.1: Overview of the PE 100 materials investigated.

Trade name	Color	Supplier	Code
BG 10050 E	black	Dow Europe	PE100-1
DGDA 2490 NT 7	white	Dow USA	PE100-2
XZ 89803.00	white	Dow Europe	PE100-3

Table 3.2: Characteristic mechanical properties of the PE-HD pipe grades investigated (E = Young's modulus, σ_Y = yield stress, ρ = density, MFI = Melt Flow Index).

Material	E [1] [MPa]	σ_y [1] [MPa]	ρ [2] [g/cm^3]	MFI [2] [g/10min]
PE 100-1	1320	26	0.96	0.23
PE 100-2	1250	26	0.95	0.3
PE 100-3	1260	25	0.95	0.24

1) measured at PCCL
2) taken from datasheets provided by the supplier

Table 3.3: Characteristic molecular properties of the PE-HD pipe grades investigated (M_n = number average molecular weight, M_w = weight or mass average molecular weight, M_z = z-average molecular weight, MWD = molecular weight distribution, SCB = short chain branching content).

Material	M_n [g/mol]	M_w [g/mol]	M_z [g/mol]	MWD	Cristallinity [%]	SCB [1/1000C]	Comono-mer
PE 100-1	10572	187340	944866	17.72	61.8/ 66.5 [1]	2.4	butene
PE 100-2	10712	226033	1008215	21.1	63.4/ 67.1 [1]	2.2	hexene
PE 100-3	12097	260233	1316807	21.51	63.5/ 67.2 [1]	2.5	butene

1) DSC, values from the 1st and 2nd heat run (heating rate: 10K/min)
2) no information available

The materials were supplied in the form of square, compression-molded plates of 15 mm thickness and 155 mm length. Fatigue crack growth tests were performed on compact type (CT) specimens with a specimen width, W, of 40 mm and cracked round bars (CRB) with a length, L, of 100 mm and a diameter, D, of 14 mm. The CT specimens were precracked by pressing a razor blade into the machined V-slot to a depth, a_0, of 12-13 mm. The CRB specimens were mounted in a lathe and circumferentially precracked to a depth, a_0, of 1.5 mm. All specimens were kept in a controlled environment (23 °C and 50 % relative humidity) for at least one week before testing.

3.2 Test device and test procedure

The fatigue crack propagation tests were performed using a servo-hydraulic closed-loop testing machine (MTS-858 Table Top, MTS System GmbH, Berlin, D) under sinusoidal load control at frequencies of 5, 10 and 30 Hz and R-ratios equal to 0.1, 0.3 and 0.5. The tests were carried out in air at room temperature (23 °C) and at a relative humidity of 50 %. Initial values of the stress intensity factor range, ΔK_{I0}, were chosen depending on the R-ratio and specimen configuration. An overview of the whole test program is given in Table 3.4.
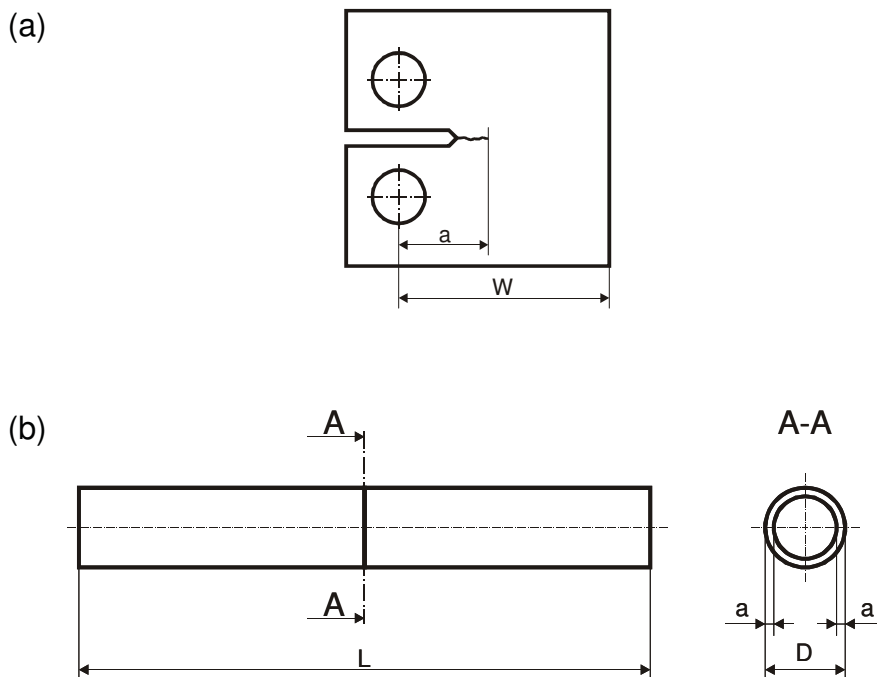
(a)

(b)

Fig. 3.1: Geometry of (a) CT and (b) CRB specimens.

Table 3.4: Test program for fatigue investigations with three different PE100 materials.

			R-ratio	
		material **specimen: initial stress intensity factor range ΔK_{I0} [MPam$^{1/2}$]**		
		0.1	**0.3**	**0.5**
Frequency [Hz]	**5**	PE100-1 PE100-2 PE100-3 CT: 1.2 CRB: 0.75	PE100-1 CT: 1.1 CRB: 0.75	PE100-1 CT: 0.9-1.0 CRB: 0.75
	10	PE100-1 CT: 1.2 CRB: 0.75	- [1]	- [1]
	30	PE100-1 CT: 1.2 CRB: 0.75	- [1]	- [1]

1) not investigated

Crack lengths were monitored with the aid of a travelling microscope mounted on a linear variable displacement transducer (LVDT). To measure the crack length in CT specimens, the machine was stopped and two residual ligament lengths, (W-a) and (W-a-r_p), were recorded by moving the travelling microscope from the back face of the specimen to the crack tip and the process zone tip (see Fig 3.2). Both values were recorded, together with the corresponding number of cycles, N. The test was then resumed. For the CRB specimens, the crack length, a, on both sides of the CRB, and the residual ligament diameter, D-2a, were measured in two ways: firstly online without stopping the machine and secondly during a short stop of the machine immediately after the online measurement.

A software package called Testware-SX (Version 4.0D) was used for the auto-mated data acquisition. Right before stopping the test, the machine recorded the current maximum and minimum loads (F_{max} and F_{min}) and the corresponding upper and lower displacements (COD_{Fmax} and COD_{Fmin}) of the crosshead over two cycles and the corresponding cycle numbers (data acquisition system 1). Another system (data acquisition system 2) was used to automatically record, every 1000 cycles, the same set of values as data acquisition system 1 without recording any infor-mation on the crack length. Tests were performed at 10 Hz and 30 Hz to
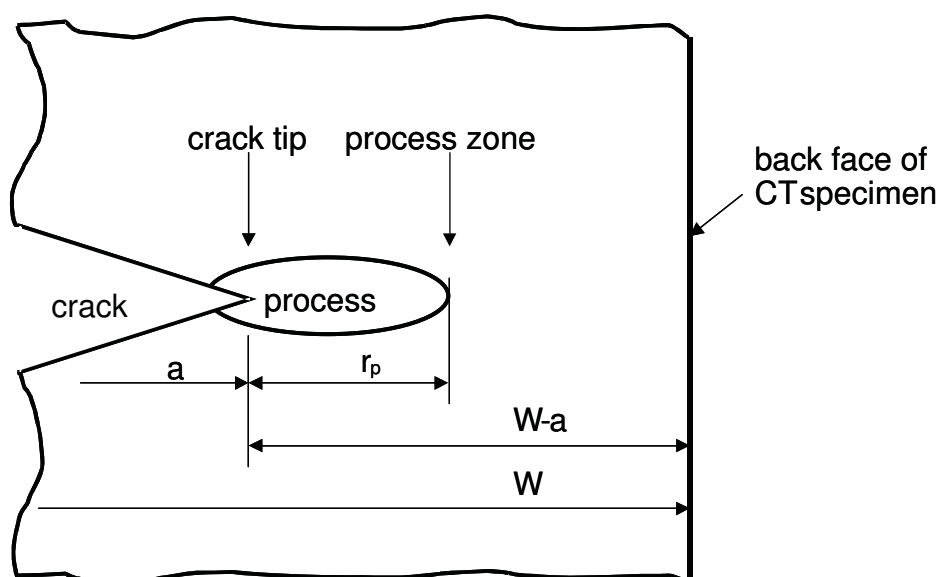

Fig. 3.2: Crack tip and process zone tip in the CT specimen.

evaluate the influence of frequency on the FCP rate and the increase in hysteretic crack tip heating by comparing the results with those obtained at 5 Hz. To investigate the temperature rise at the crack tip, an infrared camera was used (Jade 3, CEDIP Infrared Systems, Croissy Beaubourg, France), which was mounted on an xyz-positioner. Temperature measurements were taken, without interrupting the test, at three positions: (1) directly at the crack tip, (2) close to the crack tip and (3) far away from the crack tip, where (almost) no hysteretic heating was assumed (see Fig. 3.3). Each temperature measurement took about 1.5 seconds. Immediately after each measurement the test was interrupted to measure the corresponding crack length.
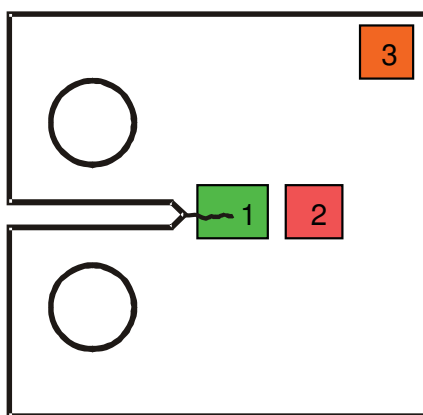

Fig. 3.3: Positions at which temperature measurements were made on CT specimens.

One objective of this investigation was the design and implementation of grips for CRB testing and the optimisation of the loading procedure for FCG testing. After problems were detected with the 1st design (see Fig. 3.4) due to slipping and asymmetrically growing cracks, the majority of the investigations reported here were performed using the 2nd design. Both grips use clamping sleeves to fix the specimen and to align the specimen along the loading axis. While four screws hold the major grip parts together in the 1st design, a single screw nut is used in the 2nd design, which should result in a more homogenous distribution of tightening torque during clamping. The 3rd design shown in Fig. 3.4 was originally developed due to slipping occurring during creep tests and was used in the last test period of the work reported here. In comparison to the former two designs, the clamping procedure was easier because the specimen was directly screwed into the grips.
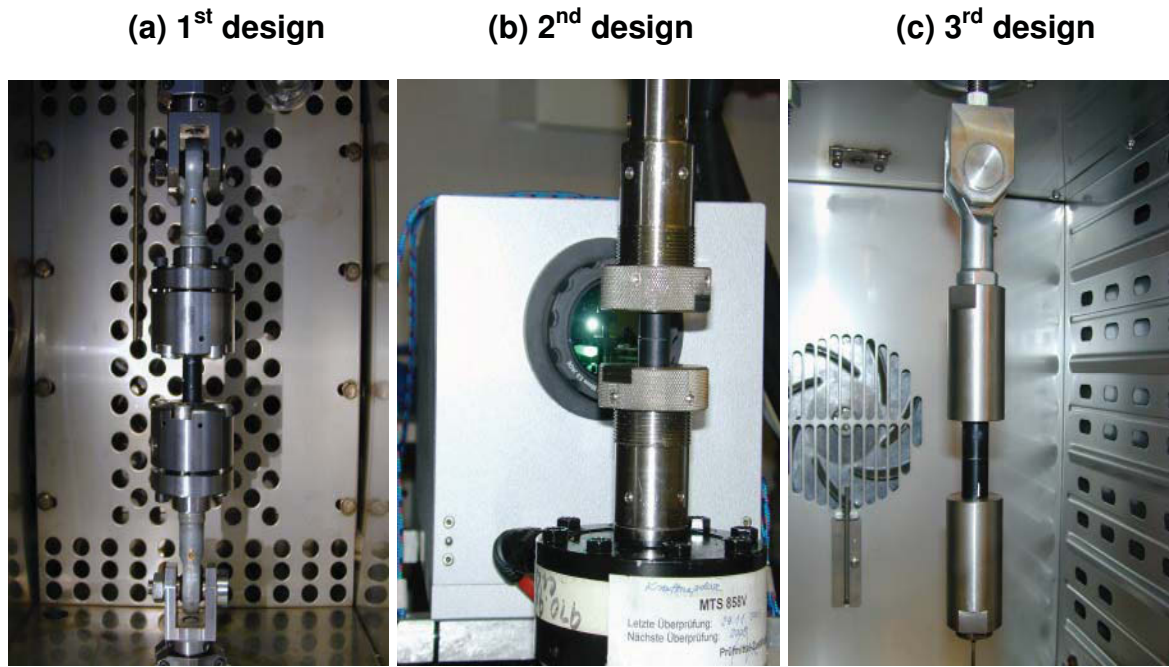
(a) 1st design **(b) 2nd design** **(c) 3rd design**

Fig. 3.4: Three different grips for testing of CRB specimens.

3.3 Data analysis and data reduction

For CT specimens the stress intensity factor range ΔK_I is given by equation 3.1;

$$\Delta K_I = \frac{\Delta P}{B \cdot \sqrt{W}} \cdot f\left(\frac{a}{W}\right)$$

(3.1)

where

$$f\left(\frac{a}{W}\right) = \frac{\left(2 + \frac{a}{W}\right)}{\left(1 - \frac{a}{W}\right)^{\frac{3}{2}}} \cdot \left[0.886 + 4.64 \cdot \frac{a}{W} - 13.32 \cdot \left(\frac{a}{W}\right)^2 + 14.7 \cdot \left(\frac{a}{W}\right)^3 - 5.6 \cdot \left(\frac{a}{W}\right)^4\right]$$

(3.2)

and ΔP is the applied load range, B is the specimen thickness, W is the specimen width, a is the crack length and f(a/W) is the non-dimensional correction function accounting for crack and specimen geometries [Hertzberg et al., 1980; Anderson 1995].

For CRB specimens the stress intensity factor range ΔK_I is given by equation 3.3,

$$\Delta K_I = \sigma \cdot \sqrt{\pi \cdot a \cdot (1 - 2\xi)} \cdot f\left(\frac{a}{D}\right)$$

(3.3)

where

$$f\left(\frac{a}{D}\right) = \frac{1.121 - 3.08\left(\frac{a}{D}\right) + 7.344\left(\frac{a}{D}\right)^2 - 10.244\left(\frac{a}{D}\right)^3 + 5.85\left(\frac{a}{D}\right)^4}{1 - 4\left(\frac{a}{D}\right) + 4\left(\frac{a}{D}\right)^2}$$ (3.4)

and σ is the nominal stress in the whole specimen (except in the ligament area), a is the crack length and D is the diameter of the specimen [Plummer et al., 2001].

To calculate the fatigue crack propagation rate from the measured crack length, two methods are used: the secant method [ISO 15850] and the incremental polynomial method [ASTM E647-00].

The secant or point-to-point method simply takes the crack growth rate as the slope of the straight line connecting two consecutive points on the a vs. N curve. Formally it can be written as:

$$\left.\frac{da}{dN}\right|_i = \frac{\Delta a}{\Delta N} = \frac{a_i - a_{i-1}}{N_i - N_{i-1}} \qquad \text{with i = 2,.....,k}$$ (3.5)

where a_i is the generic measured crack length and k is the number of available data.

The incremental polynomial method is based on the fitting of sets of (2n + 1) consecutive data points with a second order polynomial:

$$\hat{a}_i = b_0 + b_1 \cdot \left(\frac{N_i - C_1}{C_2}\right) + b_2 \cdot \left(\frac{N_i - C_1}{C_2}\right)^2$$

$$C_1 = \frac{N_{i-n} + N_{i+n}}{2}$$ (3.6)

$$C_2 = \frac{N_{i+n} - N_{i1n}}{2}$$

$$\frac{N_i - C_1}{C_2} \in [-1;1]$$

where â is the fitted value of crack length, b_0, b_1 and b_2 are coefficients obtained applying the least squares method, C_1 and C_2 are parameters used to rescale the input data in order to avoid numerical difficulties and n can be chosen to be 1, 2 or 3. If n = 3, for n+1 ≤ i ≤ k-(n+1), seven points are used for fitting: the chosen crack length datum and the previous and following three. In this case, the method is re-

ferred to as the 7-points method (see Fig. 3.5) and this is the technique used in the work presented here.

The value of $â_i$ obtained in this way takes into account seven measured crack lengths (a_{i-3}, a_{i-2}, a_{i-1}, a_i, a_{i+1}, a_{i+2}, a_{i+3}), but it does not exactly coincide with the measured a_i. However, the deviation has been found to be small enough and can be neglected.

The rate of FCP at a given number of cycles N_i can be easily calculated from the derivative of the second order polynomial (equation 3.7):

$$\frac{da}{dN}\bigg|_{â_i} = \frac{b_1}{C_2} + 2b_2 \cdot \left(\frac{N_i - C_1}{C_2^2}\right)$$

(3.7)

The corresponding ΔK_I value is calculated from equation 3.1 (CT) or 3.3 (CRB), using $â_i$ as the crack length.

From the data recorded by the machine (the actual maximum and minimum loads and the corresponding upper and lower displacements over two cycles) it is possible to deduce the specimen compliance. The compliance method allows crack size monitoring during FCP rate testing.
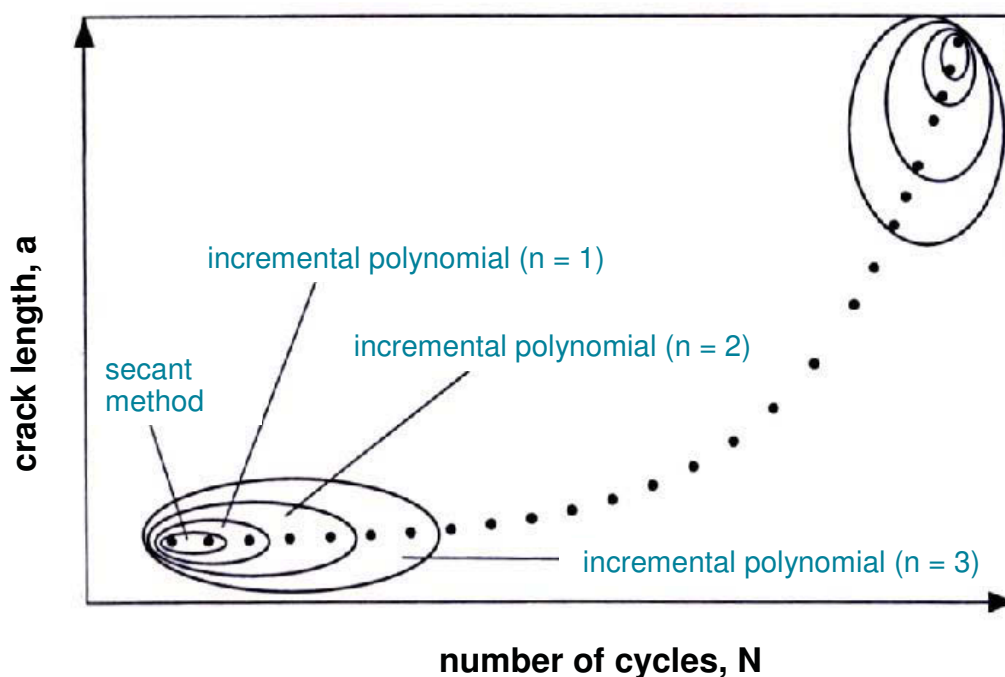

Fig. 3.5: Description of the incremental polynomial method.

Fig. 3.6 shows a plot of the measured crack length, a, vs. the specimen compliance, ΔCOD/ΔF (data from data acquisition system 1). A best-fit technique was used to obtain an expression which describes the crack length as a function of the specimen compliance. This expression was then used to calculate more crack length data simply by substituting the values of specimen compliance computed from the sets of data automatically recorded by the machine during the entire test (data from data acquisition system 2). The crack length values obtained in this way, which can be called "calculated crack lengths", can be used to calculate the FCP rate using either the secant or the incremental polynomial methods as well as the measured crack lengths. The compliance method was only used for data analysis of fatigue tests on CT-specimens.

The results of the different data reduction techniques are compared in Fig. 3.7 in a plot of crack growth rate versus stress intensity factor range for PE100-1 at room temperature. In general, the crack growth rates calculated with the secant and the incremental polynomial methods are in good agreement. The secant method is very sensitive to the scatter associated with the determination of crack length and the variation in crack speed due to inhomogeneities in material properties and therefore the range of fluctuations is relatively large.
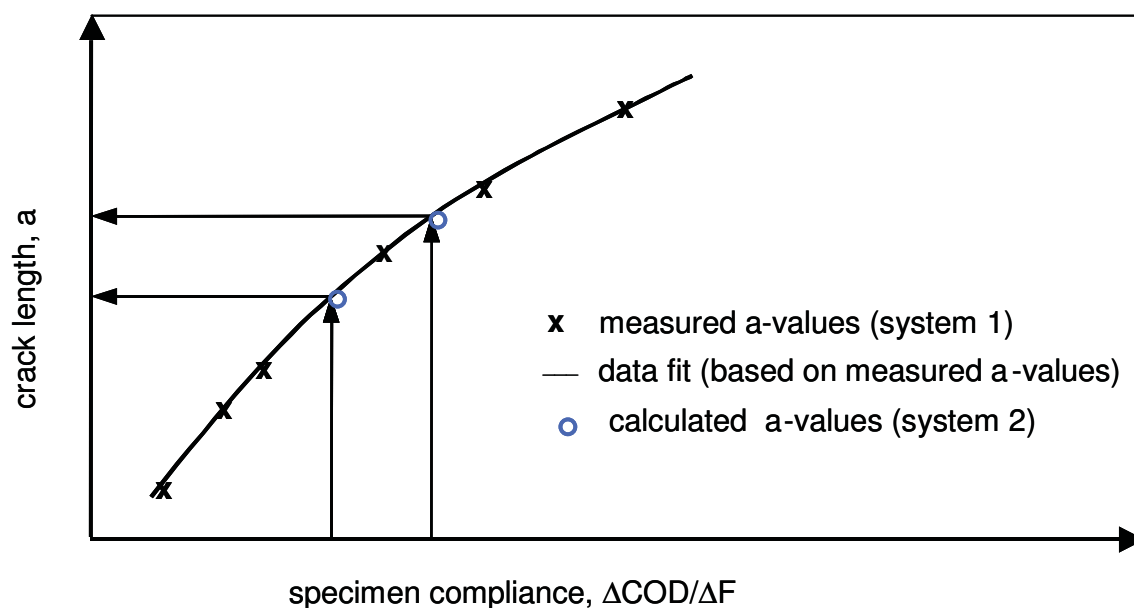

Fig. 3.6: Schematic representation of how calculated crack lengths are obtained.
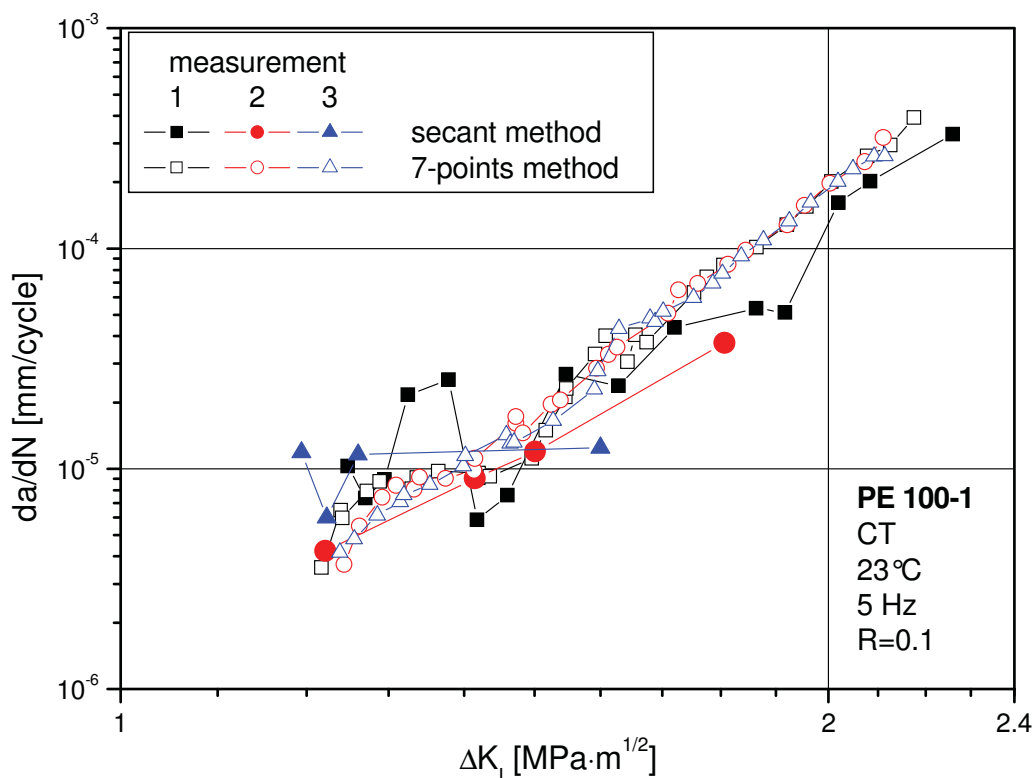
Fig. 3.7: FCG rates in PE100-1 as a function of ΔK_I (CT, 23 °C, 5 Hz, R = 0.1).

Clearly, better results are obtained with the incremental polynomial method. It accurately describes any irregularities in crack growth behavior that may occur during the test but still filters the experimental data to a degree, which produces smooth and representative crack speed curves.

When looking at the fracture surface of CT specimens, one finds that the crack propagates faster in the middle of the specimen where it is exposed to plane strain conditions, and that retarded crack growth is found in regions close to the surface, where plane stress conditions exist. Consequently the crack front over the cross-section has the shape of a thumbnail. Because of these effects, the determination of the crack length is difficult and much care is required to obtain consistent crack tip readings. Therefore, it was decided to use the position of the process zone tip to read crack length, a procedure that, at least to some degree, also corrects for crack front curvature effects. In the following investigations, all analyses of the crack growth rate for CT specimens were carried out using the crack length both excluding and including the process zone length. The results of the different analysis methods are compared in Fig. 3.8. Generally, for CT specimens there is a small shift of the values to the right, but not significantly. Results for CRB

specimens were only calculated using the physical crack tip, because the process zone was not visible during testing due to the geometry of the specimen.
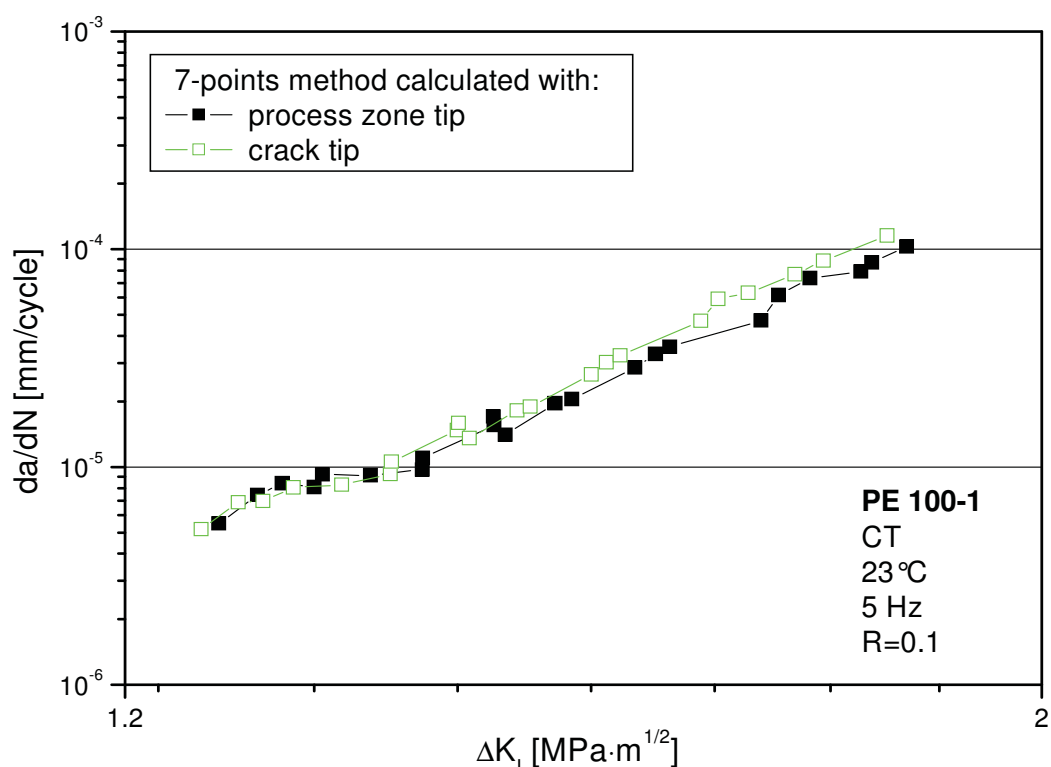

Fig. 3.8: FCG rates in PE100-1 as a function of ΔK_I (CT, 23 °C, 5 Hz, R=0.1) calculated using crack length both excluding and including the process zone length.

3.4 Fracture surface analysis

Analyses of the fracture surfaces were carried out using both a light-optical microscope (LM; Leica WILD, Heerbrugg, Switzerland) and a scanning electron microscope (SEM; Carl Zeiss, Oberkochen, Germany) for selected CT and CRB specimens. While no special preparation of the specimens was necessary for the LM investigations, the specimens for SEM investigations were coated with a nanometre layer of gold at a current of 20 mA for 400 seconds (sputter coater BAL-TEC SCD 005, BAL-TEC, Balzers, FL). The SEM had a tungsten cathode and the operating voltage was 10 kV.

4   Results and Discussion

4.1   Comparison of different PE100 pipe grade materials

The FCG behaviour of the three PE types selected was evaluated using CT specimens at an R-ratio of 0.1, 23 °C and a frequency of 5 Hz. The initial stress intensity factor, ΔK_{I0}, was chosen in such a way that the testing times did not exceed 60 hours. The tests on the PE 100 materials were therefore started at 1.2 MPa·m$^{1/2}$.

A discontinuous crack growth mechanism was characteristic for all materials investigated. Crack growth inside the specimen is higher than on the outside, which can be noted from the semi-elliptical shape of the front-line of the crack. The change from quasi-brittle to ductile behaviour and the increased ductility of the PE 100s can be seen in the pictures of the fracture surface of the CT specimens in Fig. 4.1. The arrest lines that are typical for discontinuous crack growth are quite similar in all the investigated materials and the fracture surface is characterized by an enhanced micro-ductility.

Using a scanning electron microscope at a magnification factor of 200 and 500, typical details of the fracture surface are revealed. They are compared at 2 different ΔK_I values of 1.26 and 1.62 MPa·m$^{1/2}$ in Figs. 4.2 and 4.3. Generally, the fracture surfaces reveal the remnants of voids and fibrils, the typical attributes of craze formation and breakdown. The prominent striations on the fracture surfaces are a result of the stepwise crack growth mechanism (white arrows in Fig. 4.2). With increasing values of ΔK_I, structures on the fracture surface become coarser. No significant differences in the details of the fracture surfaces could be found as a result of the material variations.

Stepwise crack propagation was observed in CT specimens and all polyethylene materials under investigation. The discontinuous character of crack growth was also well resolved in the change in crosshead displacement. A typical plot is presented in Fig. 4.4. Plateaus corresponded to the arrest periods when the crack remained stationary, a sharp increase in crosshead displacement indicates a
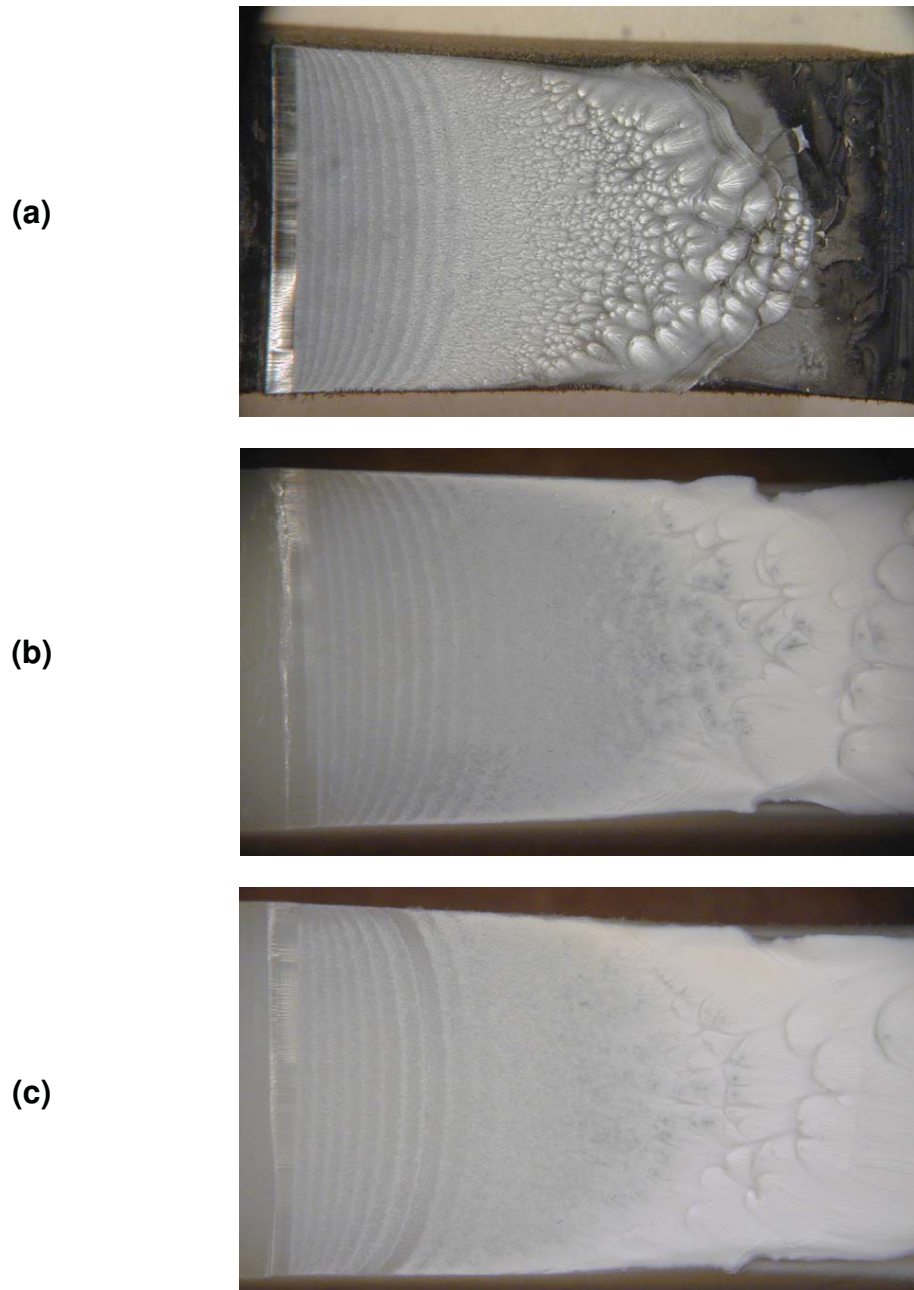
Fig. 4.1: Optical photos of the fracture surfaces of the materials investigated: (a) PE100-1, (b) PE100-2 and (c) PE100-3 (CT, 23 °C, 5 Hz, R = 0.1, ΔK_{I0} = 1.2 MPa·m$^{1/2}$).

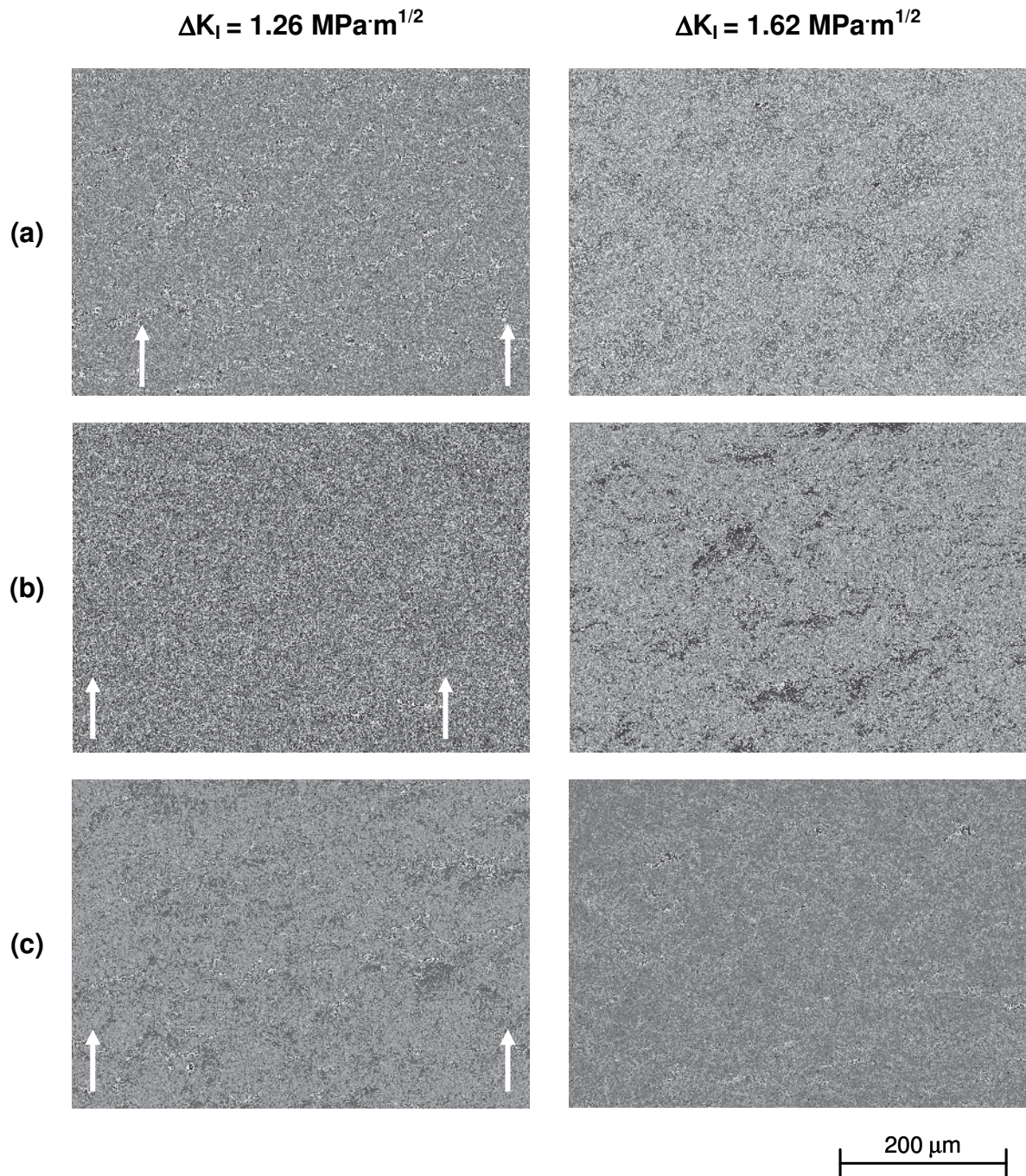$\Delta K_I = 1.26$ MPa·m$^{1/2}$ $\Delta K_I = 1.62$ MPa·m$^{1/2}$

Fig. 4.2:   SEM photos of the investigated materials (magnification factor of 200):
(a) PE100-1, (b) PE100-2 and (c) PE100-3 (CT, 23 °C, 5 Hz, R = 0.1).

$\Delta K_I = 1.26\ \text{MPa·m}^{1/2}$ $\Delta K_I = 1.62\ \text{MPa·m}^{1/2}$
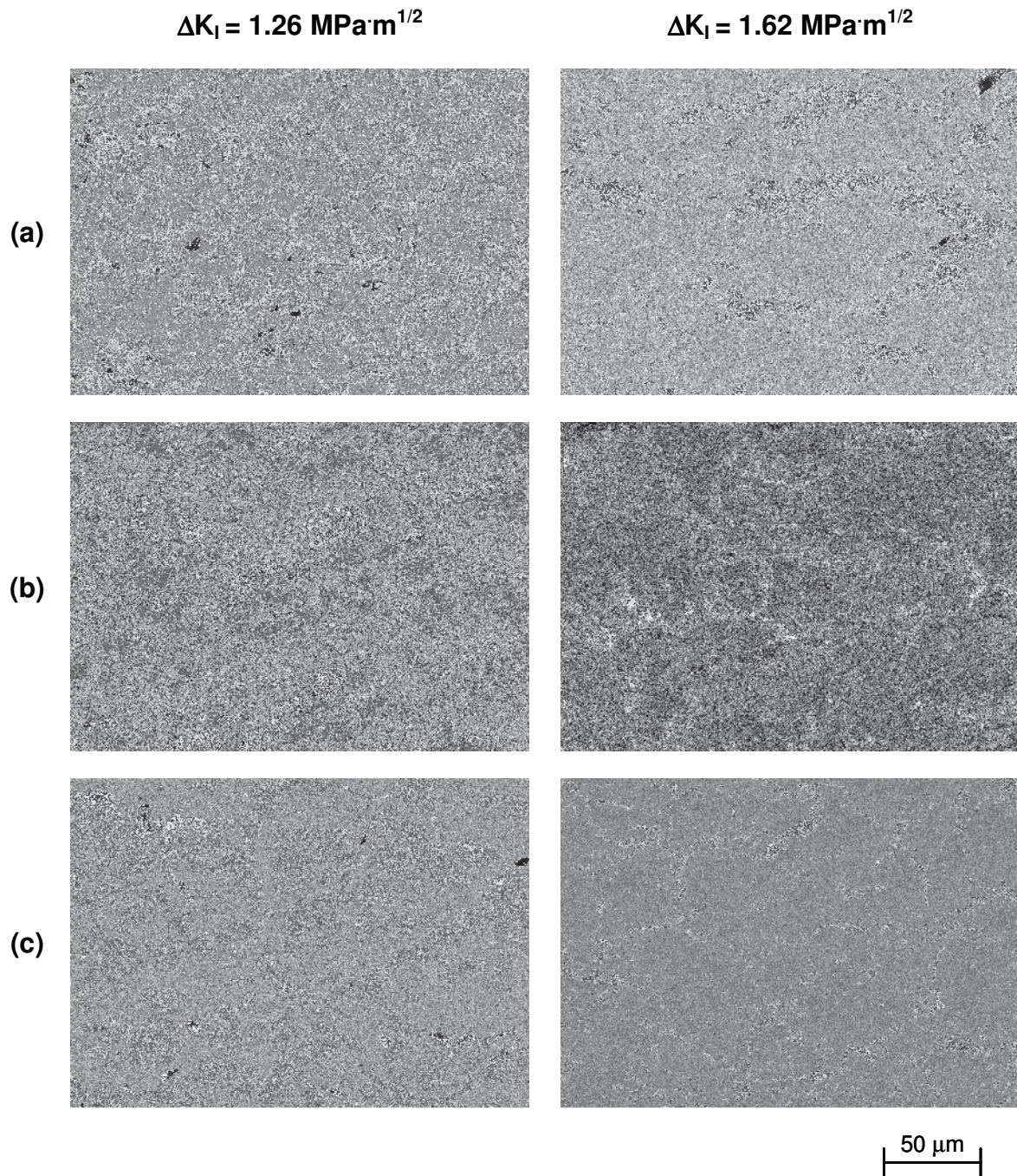

Fig. 4.3: SEM photos of the investigated materials (magnification factor of 500): (a) PE100-1, (b) PE100-2 and (c) PE100-3 (CT, 23 °C, 5 Hz, R = 0.1).

crack jump to the next arrest position. Crack initiation occurred with the first jump; an estimation of initiation is therefore possible.

The FCG data for CT specimens of the investigated materials at a given frequency of 5 Hz are shown as a function of the applied stress intensity factor range in Fig. 4.5. All pipe grades exhibited a quasi-brittle crack growth up to da/dN-values of approximately 10^{-4} mm/cycle. At higher FCG rates, LEFM concepts were no longer valid because of the increasingly ductile behavior of the three PE-HD types. Thus, no kinetic data could be determined at high da/dN-values. The FCG resistance of PE100-3 was found to be clearly the highest among the three selected polyethylenes, while the highest FCG rates were observed for PE100-1. While PE100-1 and PE100-3 differ in molecular weight, but not in the comonomer type nor significantly in the concentration of side chain branching nor even significantly in cristallinity (c.f. Table 3.3), the higher molecular weight of PE100-3 is mainly responsible for the higher FCG resistance. In the case of PE100-2, the increased FCG performance in comparison to PE100-1 could result from two material parameters: (1) the longer comonomer type (hexene instead of butene) and (2) the higher molecular weight. Considering all three polyethylenes investigated, in general the molecular weight should be the most important parameter for the increase in FCG resistance.

The time to crack initiation, t_{in}, and the time to failure, t_f, were also documented and the results are presented in Table 4.1. Comparing the absolute failure times allows the whole failure mechanism to be represented, so that possible differences in crack initiation, which are not considered in the FCG curves, can be detected. While crack initiation consumed ca. 10 to 15 % of the absolute failure times, crack propagation accounts for the major part of t_f. The ranking of materials based on the t_f values confirms the kinetic results shown in Fig. 4.5.

Table 4.1: Time to crack initiation, t_{in}, and time to failure, t_f, for FCG investigations on PE100-1, PE100-2 and PE100-3 (CT, 23 °C, 5 Hz, R = 0.1).

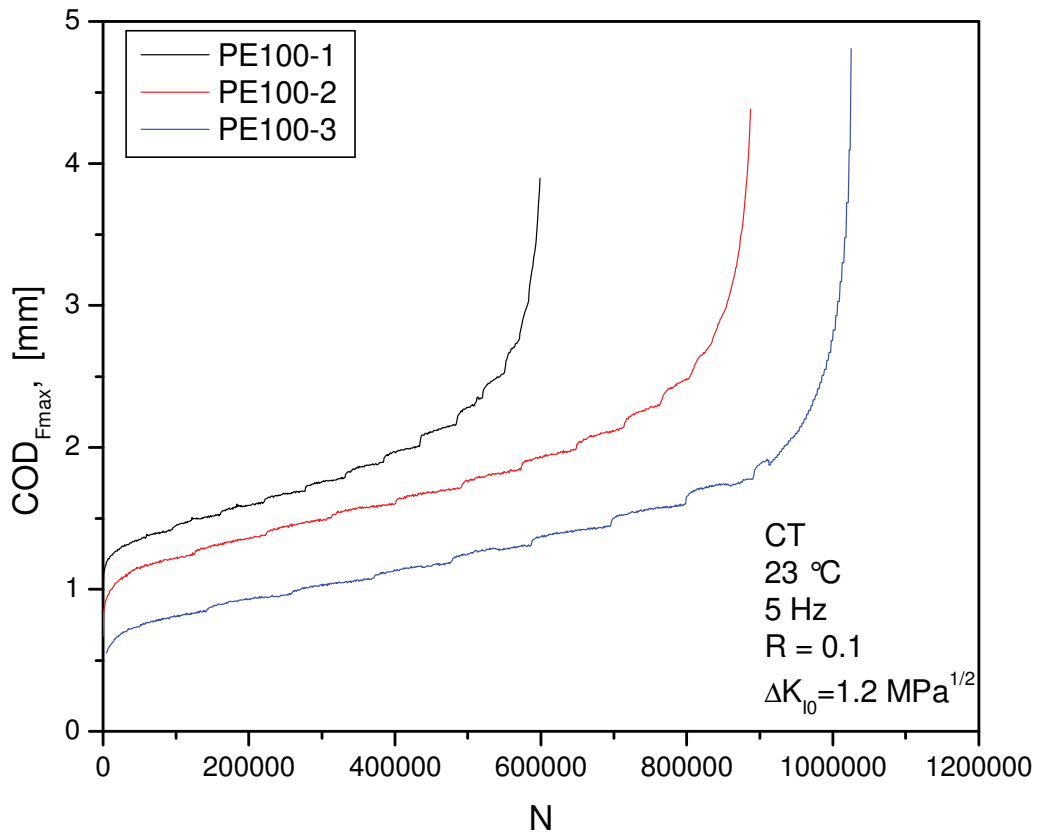| t [h]	PE100-1	PE100-2	PE100-3
t_{in}	4.2 ± 0.8	7 ± 0.8	8.3 ± 1.1
t_f	37.2 ± 5.3	49.4 ± 1.4	61.1 ± 1.1

Fig. 4.4: Crack opening displacement (COD) curves for CT specimens (23 °C, R = 0.1, ΔK_{I0} = 1.2 MPa·m$^{1/2}$).

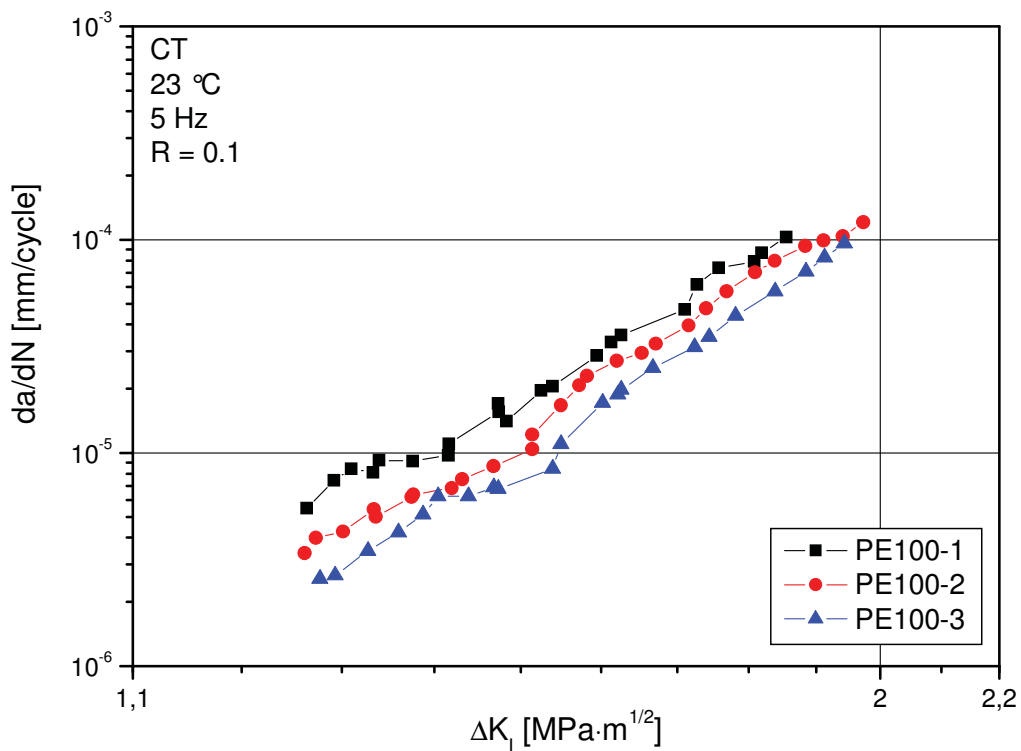**Fig. 4.5:** FCG rates of PE100-1, PE100-2 and PE100-3 as a function of ΔK_I (CT, 23 °C, 5 Hz, R = 0.1. ΔK_{I0} = 1.2 MPa·m$^{1/2}$).

4.2 Effect of specimen configuration

In order to investigate the influence of different specimen types on the FCG results, tests were also conducted at 23 °C, 5 Hz and an R-ratio of 0.1 using CRB specimens. The main reason for selecting CRB specimens was the well-defined plane strain condition in the ligament. Quasi-brittle cracks could be initiated, but it was very difficult to achieve symmetrically growing cracks. The theoretical requirement of a supremely precise transmission of force in the axial direction has not yet been properly achieved in practice. The major problem was that even very small deflections caused bending moments due to transverse forces, resulting in asymmetric crack growth.

Fig. 4.6 shows the typical fracture surfaces of CRB specimens with asymmetric crack growth at the beginning and final ductile failure. Similar to CT specimens, the fracture surface in the brittle failure regime is characterized by the typical attributes of craze formation and breakdown (voids and fibrils). The striations were visible soonest in PE100-1, however, but cannot be identified as clearly on the fracture surface of the CRB specimen as on the fracture surface of the CT specimen.

Details of the fracture surfaces shown in SEM photos were compared at the sites of crack initiation (Fig. 4.7 and 4.8). It is important to note the higher initial values of stress intensity factor for the CT specimen. While in general such comparisons should be based on equal values of stress intensity factor, this was not possible here due to the phenomenon of asymmetric crack propagation in the CRB specimens. Although there have been some attempts to calculate ΔK_I for eccentric problems [Yngvesson, 2000], a proper solution is still missing. In general, no significant differences in the details of the fracture surfaces could be found as a result of the different specimen configurations but structures on the fracture surface of the CRB specimens are finer because testing was started at lower ΔK_{I0}-values. The fracture surfaces of all three materials investigated had a similar appearance; no significant differences were found.

On the basis of the results gained so far, testing time was clearly reduced by using CRB rather than CT specimens, which could be of particular interest when ranking of materials is the goal. As a result of the problems described above, a material
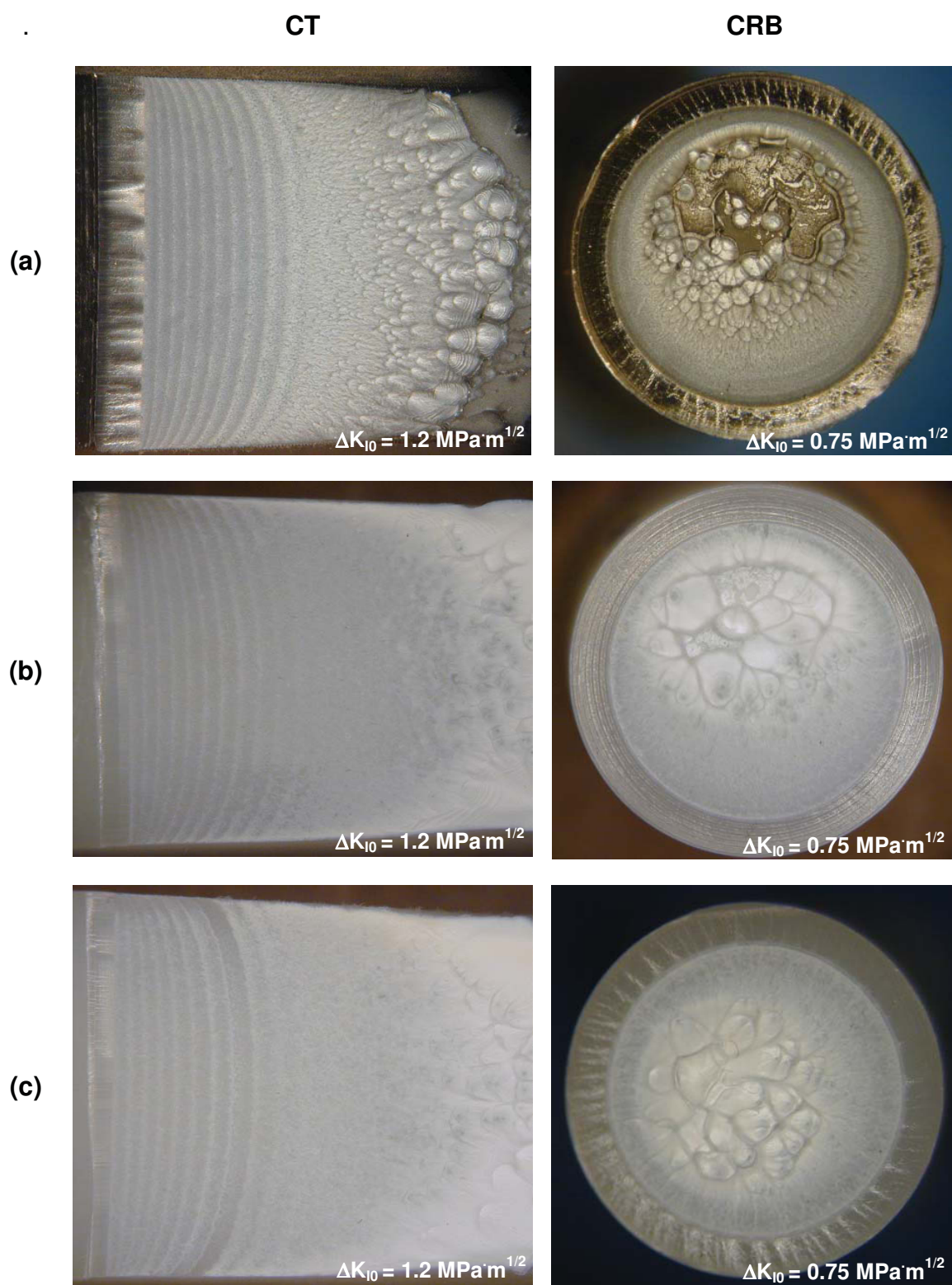
Fig. 4.6: Optical photos of the fracture surfaces of the materials investigated using CT and CRB specimens: (a) PE100-1, (b) PE100-2 and (c) PE100-3 (23 °C, 5 Hz, R = 0.1).
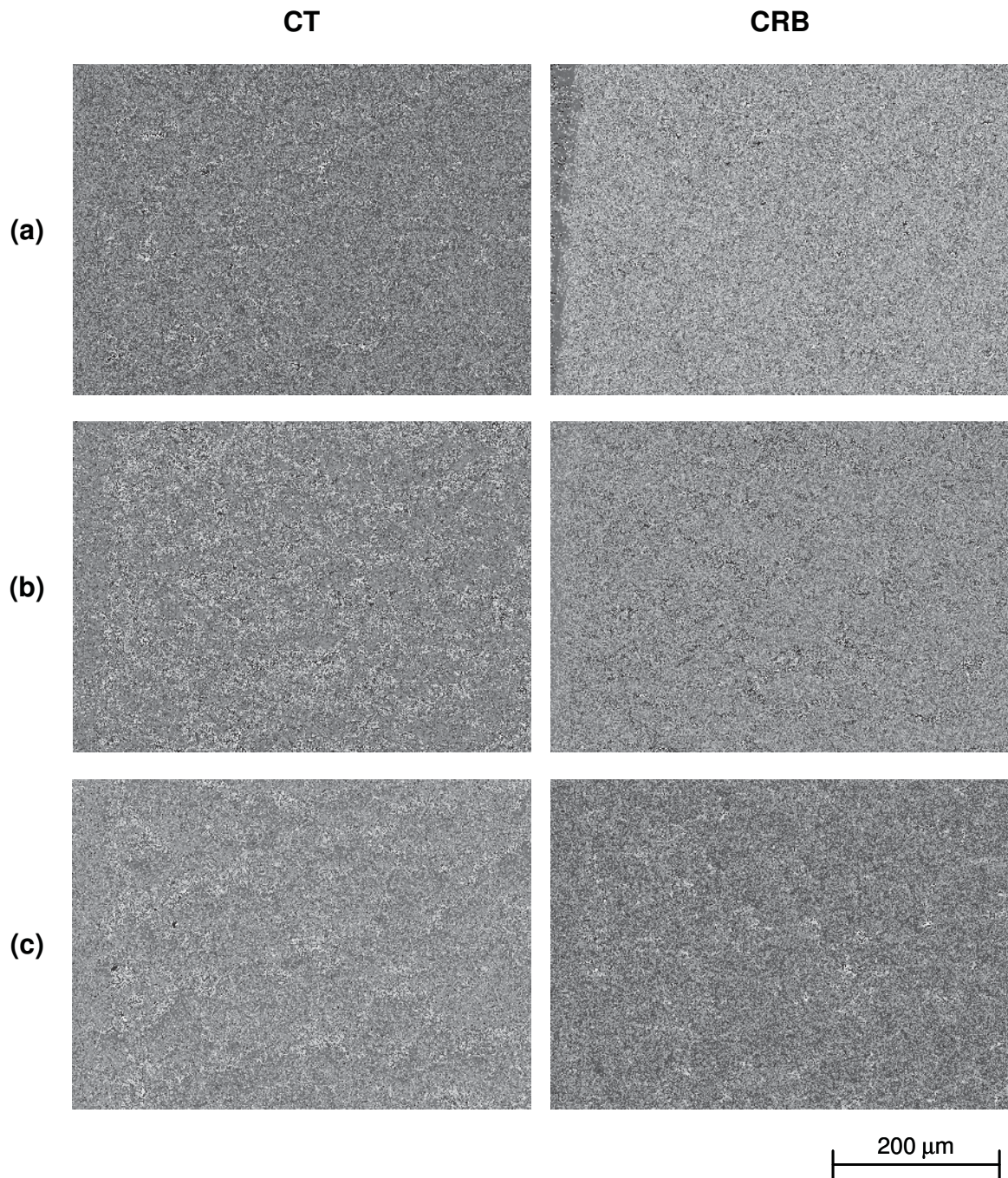
CT   **CRB**

(a)

(b)

(c)

200 µm

Fig. 4.7: SEM photos (magnification factor of 200) of (a) PE100-1, (b) PE100-2 and (c) PE100-3 in the region of crack initiation (23 °C, 5 Hz, R = 0.1).
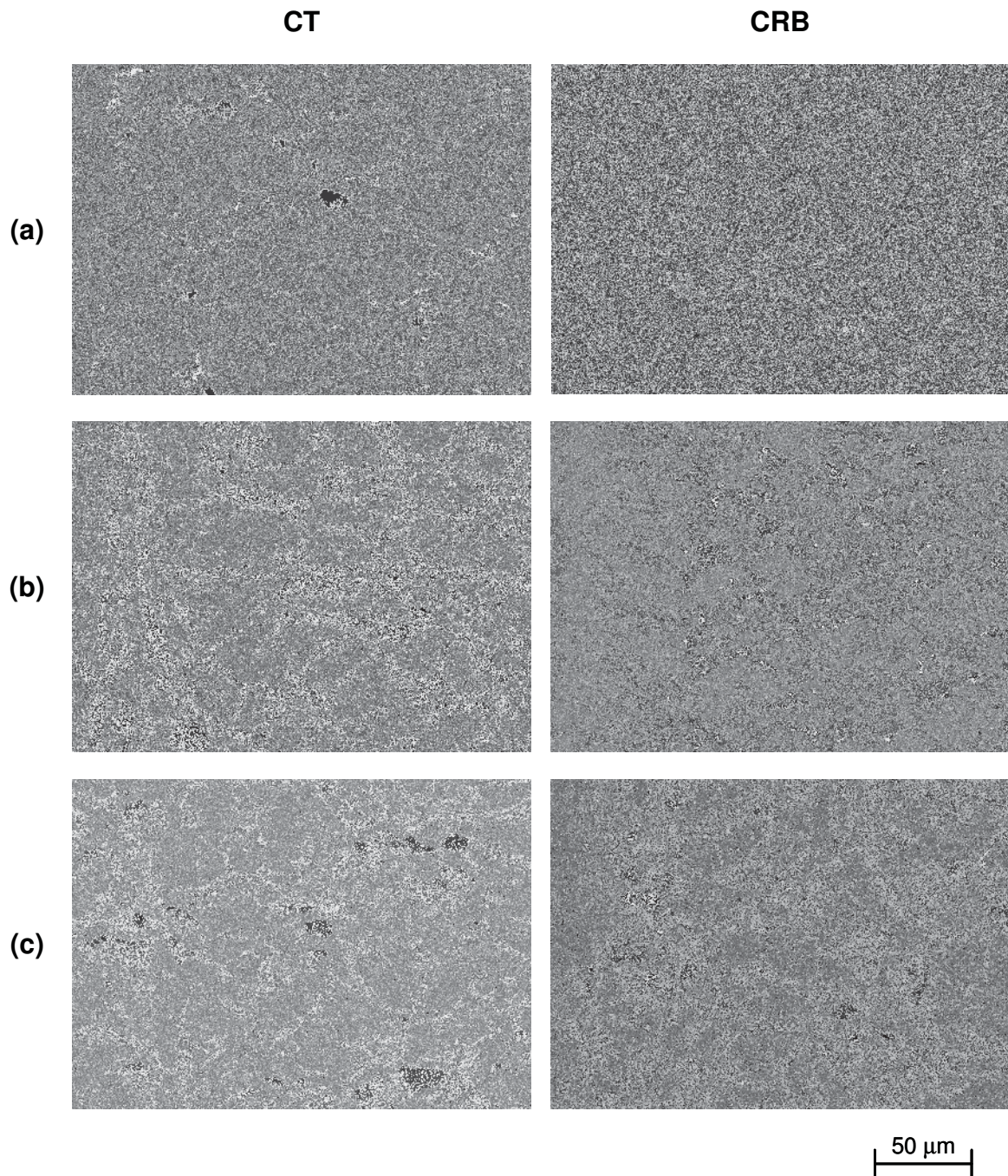
CT   **CRB**

50 µm

Fig. 4.8: SEM photos (magnification factor of 500) of (a) PE100-1, (b) PE100-2 and (c) PE100-3 in the region of crack initiation (23 °C, 5 Hz, R = 0.1).

ranking based on crack growth kinetics has not been possible so far. The materials investigated are compared on the basis of the absolute failure times in the tests (Table 4.2). In contrast to the tests on CT specimens, there are no significant differences in the t_f values of PE100-2 and PE100-3. This discrepancy can be explained as a result of the use of the different grips for CRB testing (c.f. Fig. 3.4), where a lot of optimization work had to be done leading up to this diploma thesis. The best grips (design 3 in Fig. 3.4) could only be used during the last test period. Unfortunately, earlier tests could not be reproduced due to a lack of specimens. Nevertheless, the following conclusions can be made: One great advantage of CRB testing is the reduction in testing time. Although the tests with CRB specimens were started at a lower initial stress intensity factor than the tests with CT specimens (0.75 MPa·m$^{1/2}$ compared to 1.2 MPa·m$^{1/2}$), the testing times dropped to approximately half. Regarding the procedure of grip optimization, the material ranking is in good agreement with the failure times determined using CT specimens. It is interesting to note that the CRB testing methodology has been further developed and implemented as a powerful tool for material ranking [Haager et al., 2006].

In Fig. 4.9, COD data from CT and CRB specimens are compared. Stepwise crack propagation was observed for CT specimens under investigation. The discontinuous character of the crack growth is illustrated well by the change in crosshead displacement. From the COD data of the investigated CRB specimens it could not be clearly concluded whether crack growth was continuous or step-wise, because changes in COD couldn't be properly detected due to the coarse resolution of the crosshead displacement. Other investigations using extensometers for finer resolutions have clearly illustrated that discontinuous crack

Table 4.2: Time to failure, t_f, for FCG investigations on PE100-1, PE100-2 and PE100-3 using CT and CRB specimens (23 °C, 5 Hz, R=0.1).

	Material	**CT** ΔK_{I0} = 1.2 MPa·m$^{1/2}$	**CRB** ΔK_{I0} = 0.75 MPa·m$^{1/2}$
	PE100-1	37.2 $\pm$ 5.3	18.9 $\pm$ 2.4
t_f [h]	PE100-2	49.4 $\pm$ 1.4	35 $\pm$ 3.8
	PE100-3	61.1 $\pm$ 1.1	32.5 $\pm$ 1.5

growth also occurs in CRB specimens [Haager et al., 2005b; Haager et al., 2006; Hiesch, 2005; Hiesch et al., 2005].

In Fig. 4.10, FCG curves are compared for three different CRB and CT specimens of PE100-1. Due to the problem of asymmetric crack propagation, the ΔK_I values calculated for CRB specimens represent some kind of average values. It is obvious that the scatter in the results is much higher for the CRB specimens. This can be explained in two ways. On the one hand, asymmetric crack growth makes it very difficult to identify the right crack length. On the other hand, the high gradient of ΔK_I in these load-controlled tests (with constant load peaks) makes the generation of FCG data rather difficult. Moreover, it is obvious from Fig. 4.10 that the FCG data from the CRB specimens is shifted to higher crack growth rates. Based on LEFM, FCG should be independent of the specimens used. Apparently, the pronounced plane strain conditions in CRB specimens are responsible for the decrease in FCG resistance compared to CT specimens, where plane stress conditions prevail at least at the specimen surfaces. Furthermore, more investigations will be necessary to clarify the possible influence of asymmetric crack propagation on the differences in kinetic data.
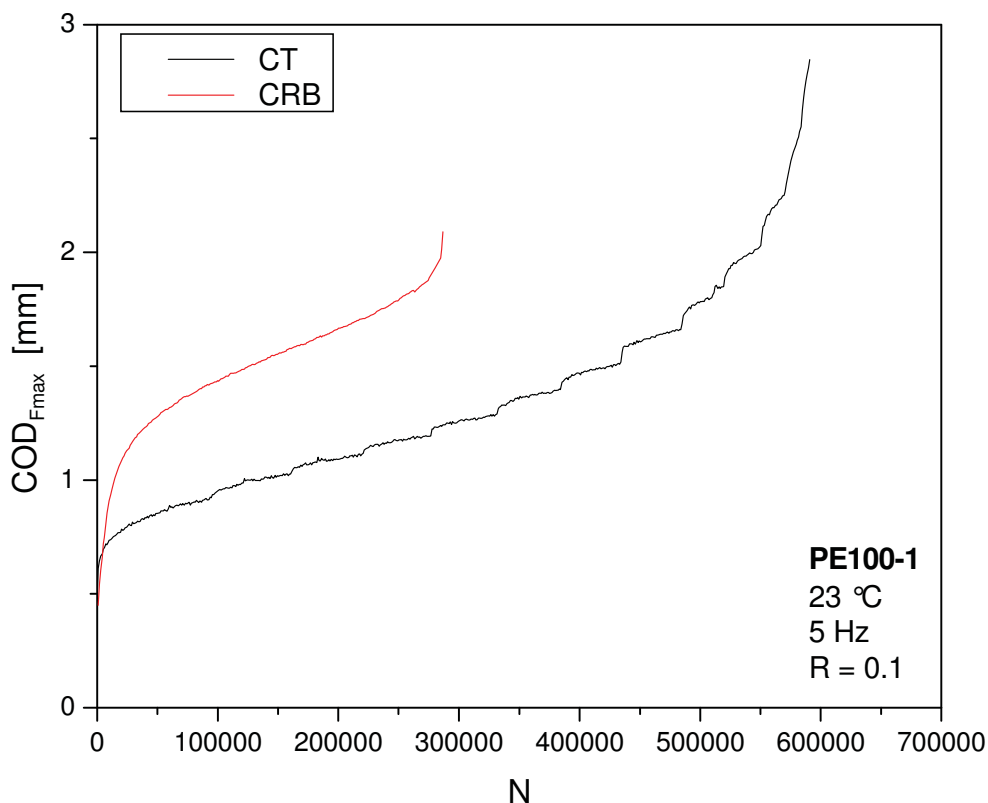

Fig. 4.9: Crack opening displacement (COD) curves from CT specimens (ΔK_{I0} = 1.2 MPa·m$^{1/2}$) and CRB specimens (ΔK_{I0} = 0.75 MPa·m$^{1/2}$) (23 °C, 5 Hz, R = 0.1).
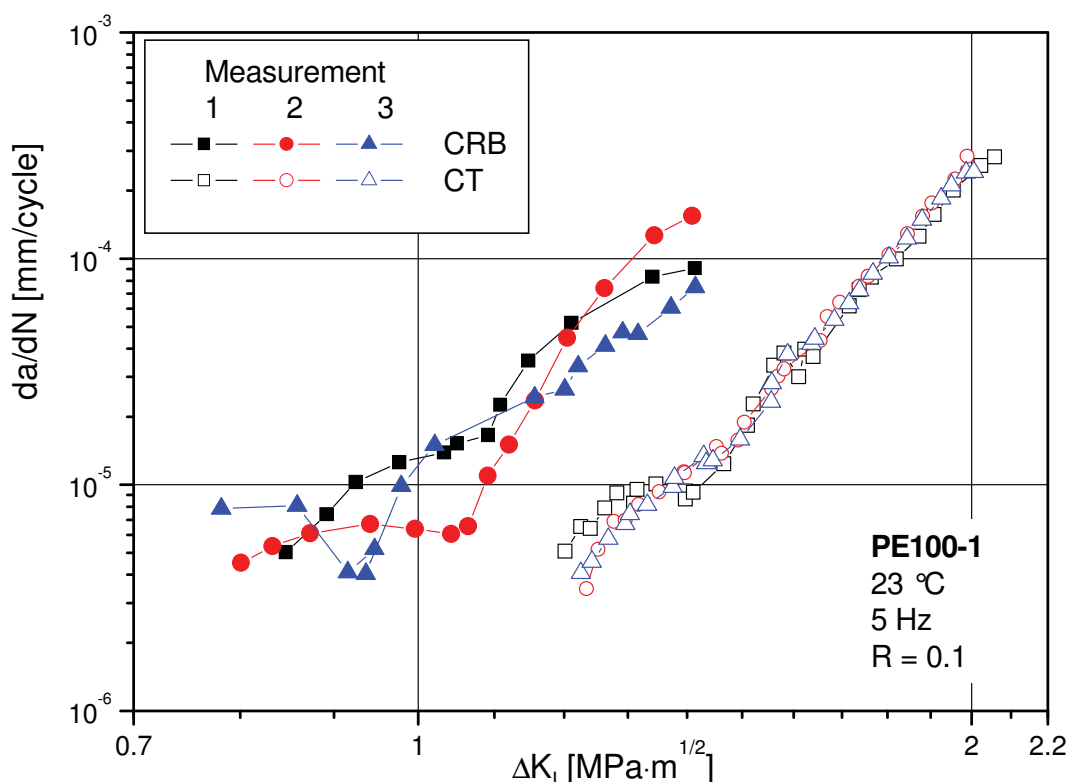
Fig. 4.10: FCG rates in PE100-1 as a function of ΔK_I, using CT and CRB specimens (23 °C, 5 Hz, R = 0.1).

4.3 Effect of frequency

In order to investigate the effects of frequency on FCG, resistance tests were conducted using CT and CRB specimens of PE100-1 at 5, 10 and 30 Hz. Typical fracture surfaces of specimens tested at the different frequencies are compared in Fig. 4.11, microscopic details from the SEM are shown in Figs. 4.12 to 4.15. For the CT specimens, striations on the fracture surfaces document the stepwise crack growth mechanism. While no clear differences in the details of the fracture surfaces of the CT specimen could be found as a result of the variations in frequency, CRB specimens tested at 10 Hz showed no striations and the area of quasi-brittle crack propagation was smaller than at 5 Hz. In the case of 30 Hz, predominantly ductile failure was observed, which is documented by the coarser and more blurred structures. This fact is assumed to be a result of increased hysteretic heating effects at the crack tip.

Due to the curved geometry of CRB specimens, the temperature increase, ΔT, at the crack tip could only be measured using an infrared camera for the CT

specimen (Fig. 16a). Similar increases in temperature at the crack tip from approximately 2 °C after crack initiation to 7 °C in the relevant ΔK_I range occurred at both 5 and 10 Hz. At 30 Hz, crack-tip heating was distinctly increased with temperatures from 5 °C to about 20 °C. In addition, Fig. 4.16 shows the temperature rise at another two positions in the CT specimen for 5, 10 and 30 Hz (c.f. Fig. 3.3), close to the crack tip (Fig. 16b) and far away from the crack tip where (almost) no hysteretic heating was assumed (Fig. 16c). For all frequencies investigated it can be seen that (almost) no increase in temperature occurred at the position far away from the crack tip. While a small temperature increase up to ca. 3 °C was observed close to the crack tip for frequencies of 5 and 10 Hz, significantly higher changes of temperature in the range of 3 to 8 °C occurred at 30 Hz.

When examining the FCG data in Fig. 4.17, it becomes apparent that with in-creasing test frequency there is a noticeable increase in crack growth resistance in CT specimens in the low crack-growth regime, while in CRB specimens no differ-ences could be found because of the large scatter band. At higher crack-growth rates, the curves coincide. This frequency sensitivity of FCG in polymers can be explained in terms of the effects of changes in strain rate on the dynamic modulus and by the effects of localized heating, which blunts the crack tip (beneficial), versus generalized heating, which leads to an overall decrease in specimen stiff-ness (detrimental).

In discussing the effects of hysteretic heating on FCG behavior, it must be taken into account that local changes in the material parameters like Young's modulus and yield stress in front of the crack tip may affect FCG rates [Lang, 1984]. Thus, due to the importance of other factors affecting possible changes in fatigue crack growth rate with frequency (local strain rate, loading rate, area under force-time-curve, creep effects [Lang, 1984; Parsons et al, 2000]), the behavior observed at higher FCG rates in Fig. 4.23 can be explained by a compensation of all conflicting processes.

Based on these measurements, the influence of test frequency on the FCG be-havior in the investigated PEs can be explained in the following way: In the low ΔK_I range a higher frequency leads to lower crack growth rates because of the higher dynamic modulus of the material under these test conditions and the enhanced

crack-tip blunting due to increased localized heating. The coinciding curves at higher ΔK_I values can be interpreted in terms of the increasing importance of a modulus drop due to cross-specimen heating at higher test frequencies and resulting in higher crack growth rates.

The time to failure, t_f, was also documented and the results are presented in Table 4.3. It is not surprising that test times were reduced at increased frequency. However it must be borne in mind that the heating effects must be considered in all discussions of this aspect (c.f. Fig. 4.16). Therefore, the test results are also presented as the number of cycles to failure, N_f. Compared to the test carried out at 5 Hz, the N_f values significantly increased in the test at 30 Hz. That is in good correlation with the kinetic data presented in Fig. 4.17.

Additionally, independent of frequency, testing times were significantly reduced when CRB specimens were used instead of CT specimens. This is especially remarkable due to the lower initial stress intensity factor ranges in the tests with CRB specimens.

Table 4.3: Time to failure, t_f, and number of cycles to failure, N_f, for FCG investigations on PE100-1 using CT and CRB specimens (23 °C, R = 0.1).

	f [Hz]	CT $\Delta K_{I0} = 1{,}2$ MPam$^{1/2}$	CRB $\Delta K_{I0} = 0.75$ MPam$^{1/2}$
t_f [h]	5	37.2 ± 5.3	18.9 ± 2.4
	10	21.5	9
	30	7.8	4.3 ± 1.4
N_f	5	672.000	339.000
	10	775.000	324.000
	30	842.000	461.000
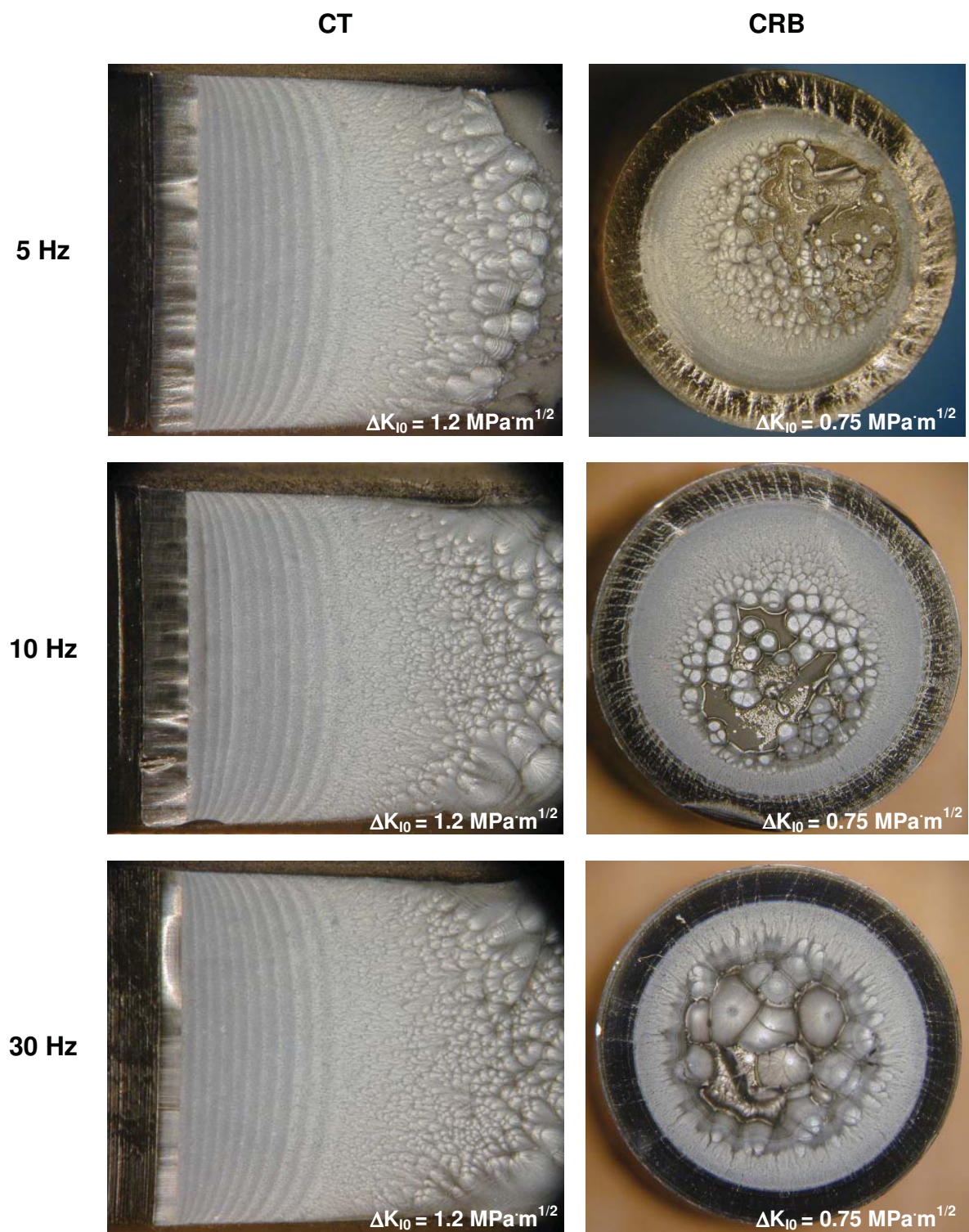
Fig. 4.11: Optical photos of PE100-1 after testing at various frequencies (23 °C, R = 0.1.)

CT

$\Delta K_I = 1.26$ MPa$\cdot$m$^{1/2}$

CRB

$\Delta K_I = 0.87$ MPa$\cdot$m$^{1/2}$

5 Hz

10 Hz

30 Hz

200 µm

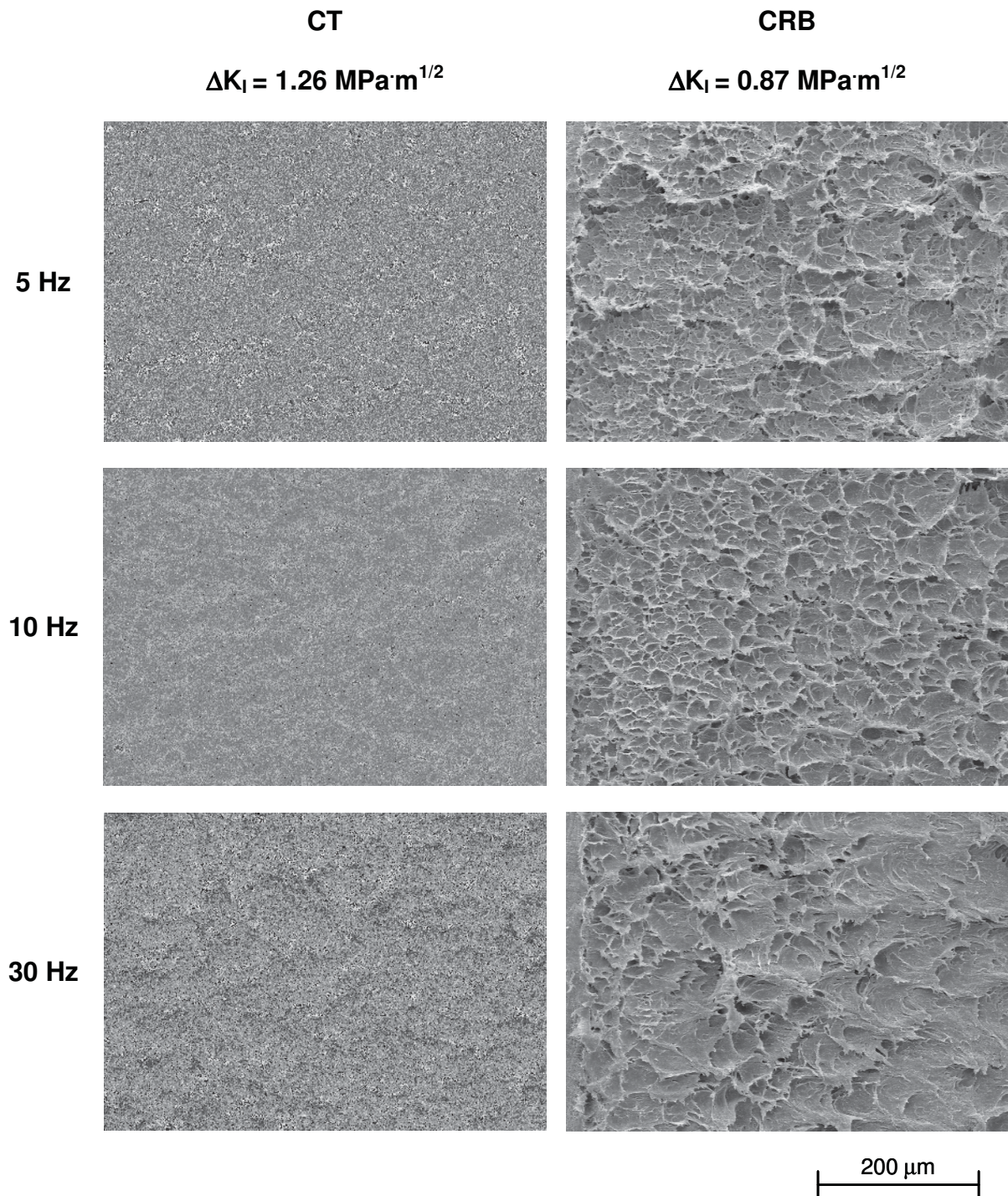**Fig. 4.12**: SEM photos of PE100-1 (magnification factor of 200) after testing at various frequencies (23 °C, R = 0.1).

CT

$\Delta K_I = 1.26$ **MPa·m$^{1/2}$**

CRB
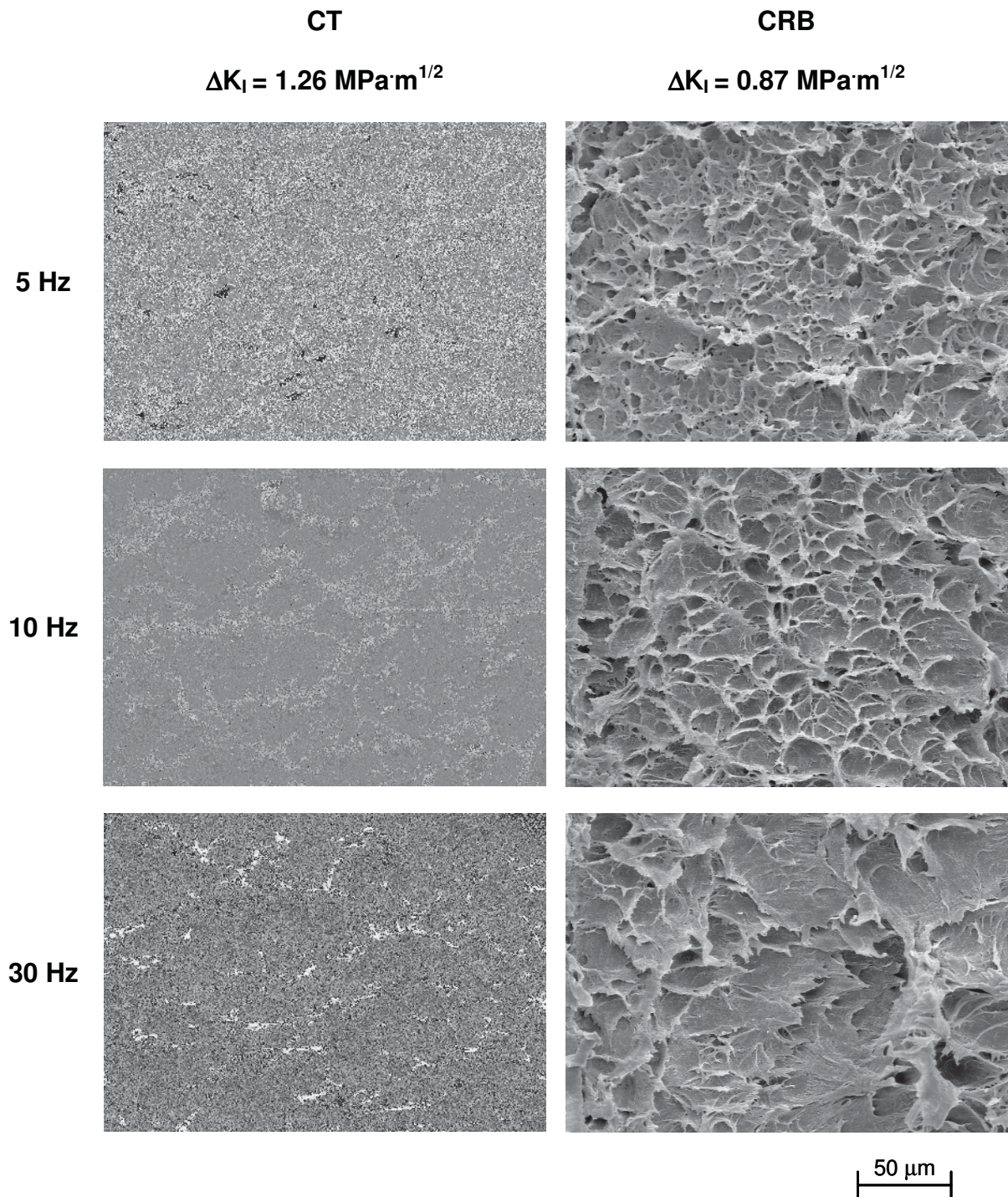
$\Delta K_I = 0.87$ **MPa·m$^{1/2}$**

5 Hz

10 Hz

30 Hz

50 µm

Fig. 4.13: SEM photos of PE100-1 (magnification factor of 500) after testing at various frequencies (23 °C, R = 0.1).

CT

CRB

$\Delta K_I = 1.62\ \text{MPa·m}^{1/2}$

$\Delta K_I = 1.1\ \text{MPa·m}^{1/2}$

5 Hz

10 Hz

30 Hz

200 µm

Fig. 4.14: SEM photos of PE100-1 (magnification factor of 200) after testing at various frequencies (23 °C, R = 0.1).

CT

$\Delta K_I = 1.62 \ MPa \cdot m^{1/2}$

CRB

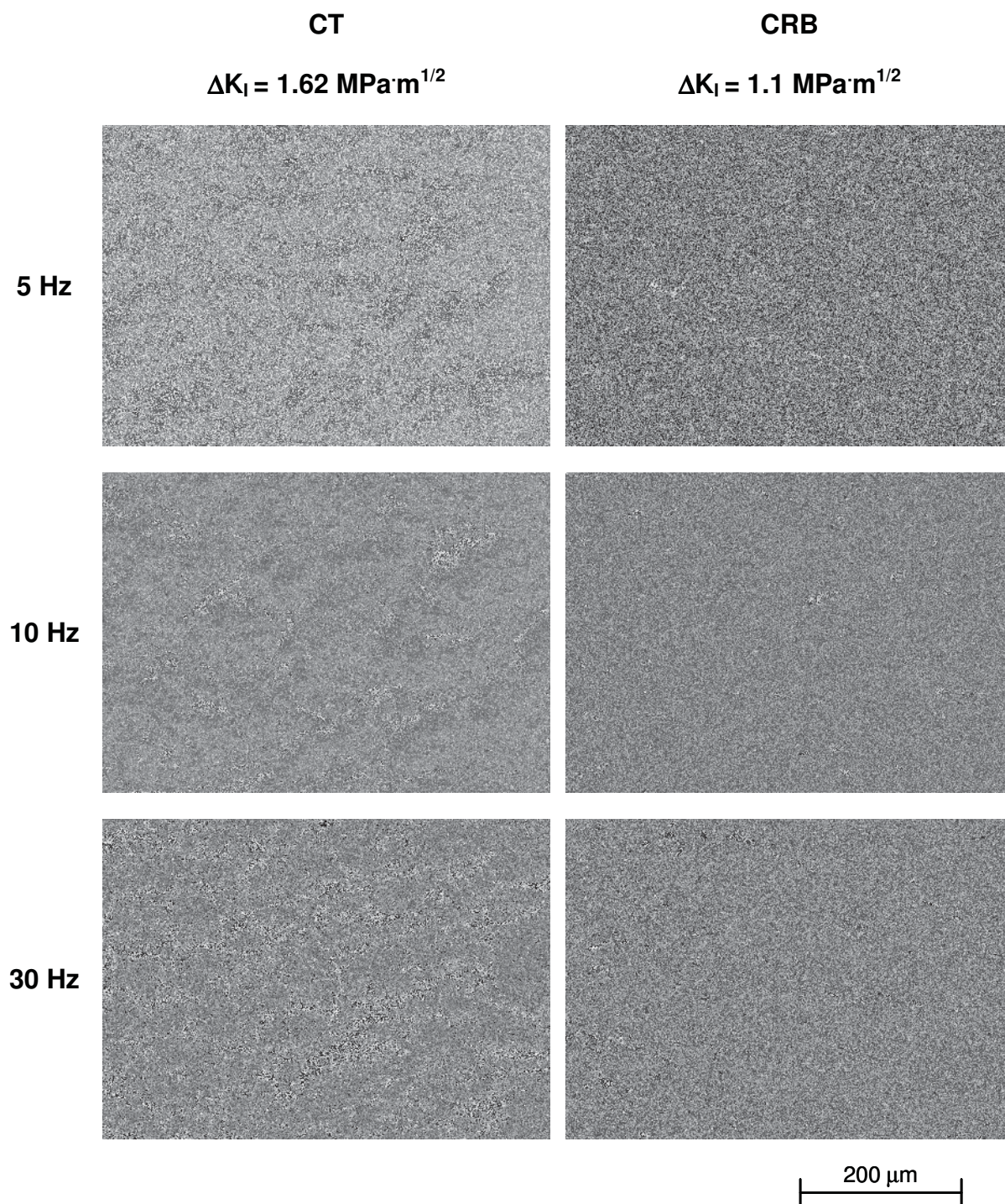$\Delta K_I = 1.1 \ MPa \cdot m^{1/2}$
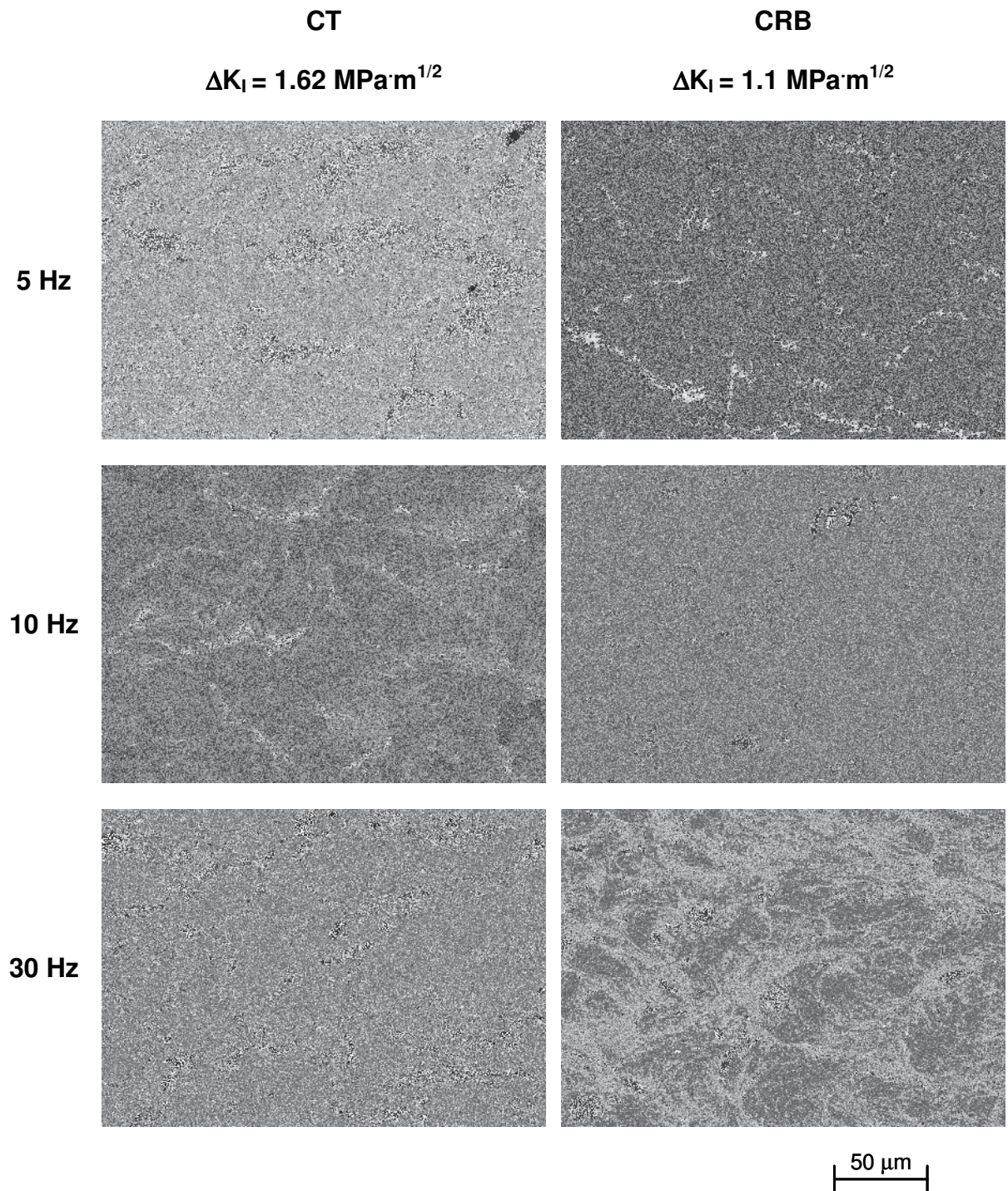
5 Hz

10 Hz

30 Hz

50 µm

Fig. 4.15: SEM photos of PE100-1 (magnification factor of 500) after testing at various frequencies (23 °C, R = 0.1).
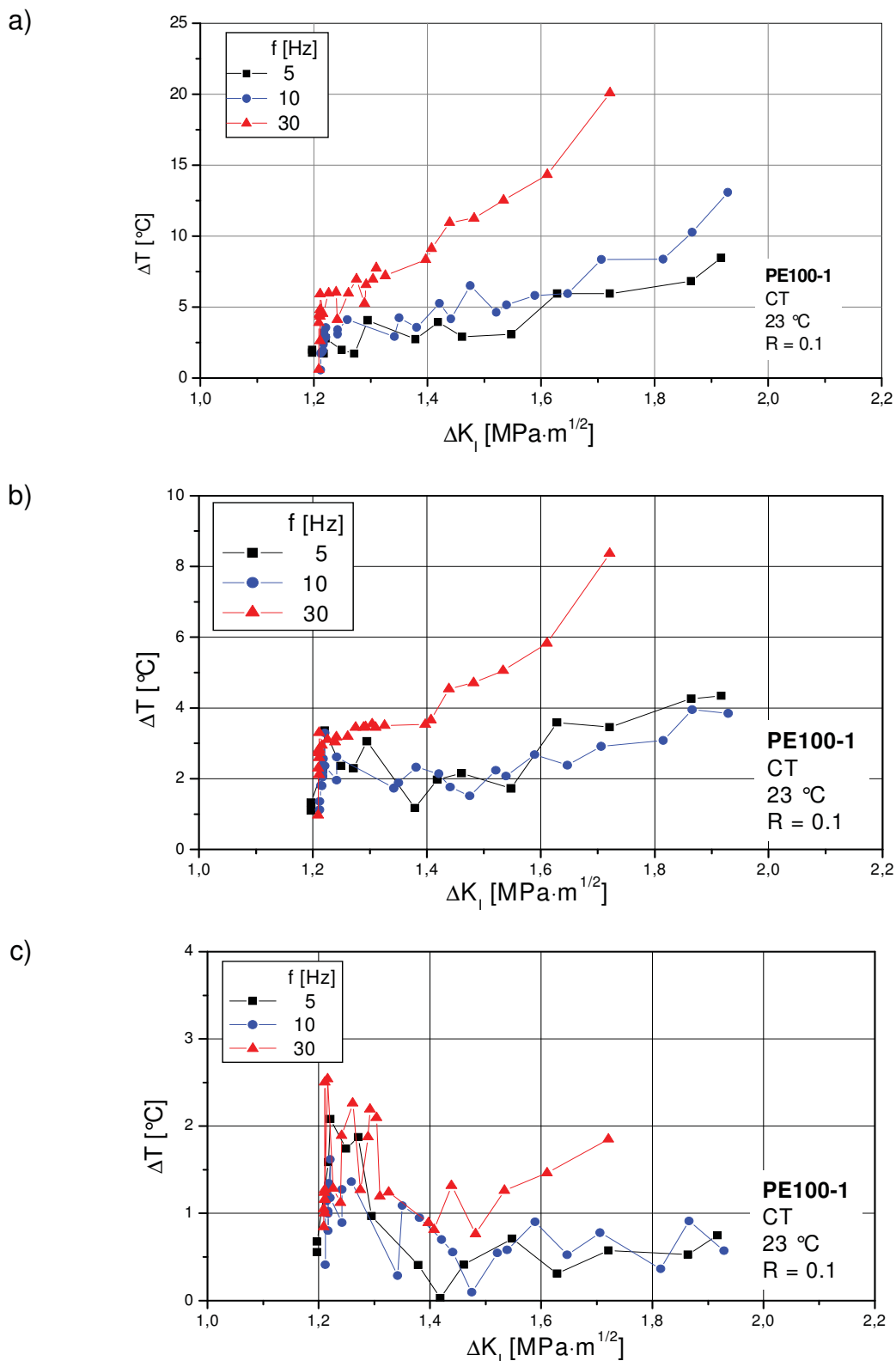
Fig. 4.16: Temperature rise at three different positions in the CT specimen as a function of ΔK_I (23 ℃, $R = 0.1$, $\Delta K_{I0} = 1.2$ MPa·m$^{1/2}$); (a) at the crack tip, (b) close to the crack tip and (c) far away from crack tip.
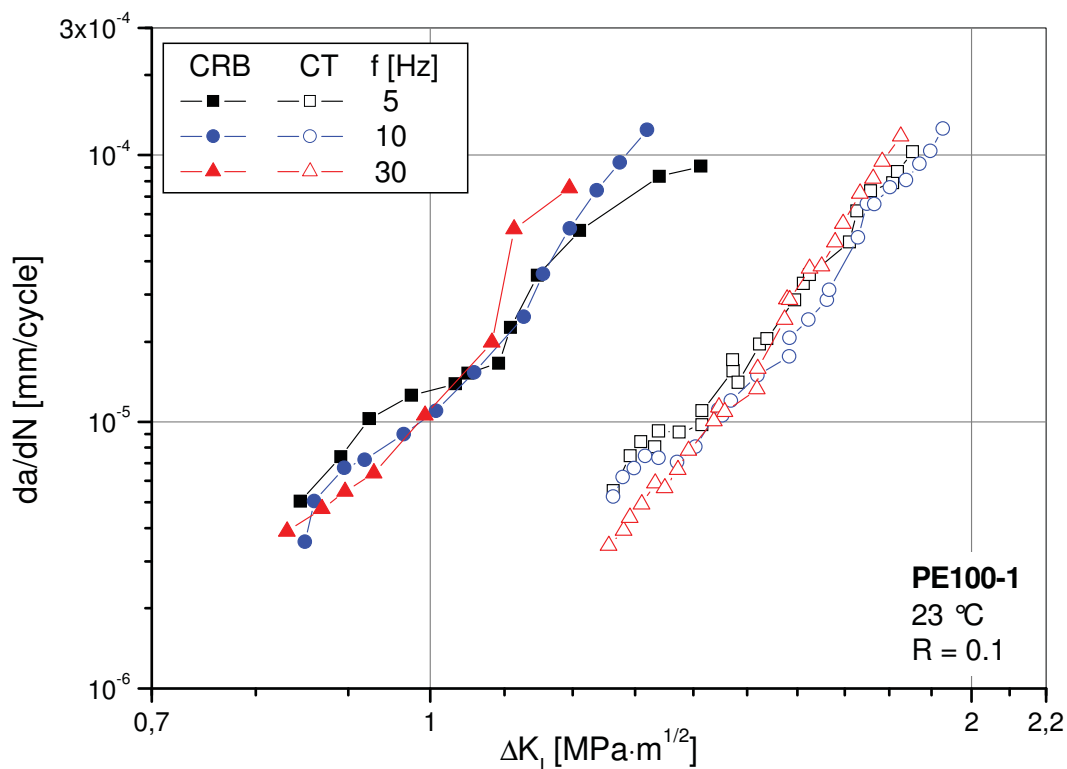
Fig. 4.17: FCG rates as a function of ΔK_I in PE100-1 using CT and CRB specimens at various frequencies (23°C, R = 0.1).

4.4 Effect of the R-ratio

The pronounced influence of the R-ratio on the micro-morphology of the fracture surface of the investigated PE in Fig. 4.18, where there are more highly stretched fibrils as the R-ratio is increased, apparently reflects the corresponding increase in craze-zone dimensions. At constant ΔK_I values, higher R-ratios are assumed to lead to more extended process zone dimensions, which act to blunt the crack and result in an increased tendency for strain energy dissipation thus acting to reduce crack growth rates, as observed for example by [Lang et al., 2004; Pinter et al., 2002c]. While equal process zone dimensions are assumed at constant K_{Imax} values, detailed examinations in [Balika et al., 2004; Fuchs, 2006] have shown that process zone lengths may even be lower at higher levels of R-ratio at constant K_{Imax} values through the whole thickness direction. In all tests, and especially for CRB specimens, the fracture surfaces reflect a transformation from quasi-brittle failure to ductile failure with increasing R-ratio, which is also documented in the microscopic details of the crack initiation regions shown in Figs. 4.19 and 4.20. FCG data for PE100-1, illustrating the effects of variations in R-ratio at a given fre-

quency for CT specimens, are shown as a function of the applied stress intensity factor range in Fig. 4.30a. In terms of ΔK_I, the fatigue crack growth rates were found to strongly depend on the R-ratio. In the case of R = 0.5, the validity of LEFM was limited to low da/dN-values and low ΔK_I-values. Since a shift of the curve to the left was observed with increasing R-ratio, FCG rates in PE100-1 are not only controlled by the stress intensity factor range at the defined test parameters, but also by the maximum stress intensity factor and/or the mean stress intensity factor (see also Fig. 4.30b), which is in good agreement with results presented in [Pinter et al, 2002; Bucknall et al, 1985; Parsons et al, 1999 and 2000]. There may be a tendency for higher crack growth rates at higher R-ratios as a result of more creep crack extension associated with the higher maximum and mean stress intensity levels [Pinter et al., 2002, Lang et al., 2003].

The time to crack initiation, t_{in}, and the time to failure, t_f, were also documented and the results are presented in Table 4.4. In the case of CT specimens, the t_{in} values increased at higher R-ratios due to increasing ΔK_{I0} values; the testing times were in the range of 37 to 44 h. In the case of CRB testing, no information about t_{in} was available for reasons discussed in section 4.2 (c.f. Fig. 4.9). In the tests where quasi-brittle crack propagation was achieved (R = 0.1 and partly R = 0.3) the CRB specimens failed after ca. 20 h, whereas ductile failure occurred after just 1 h (R = 0.5).

Table 4.4: The time to crack initiation, t_{in}, and the time to failure, t_f, for FCG investigations on PE100-1 with CT and CRB specimens (23 °C, 5 Hz).

	CT			CRB		
R	0.1	0.3	0.5	0.1	0.3	0.5
ΔK_{I0} [MPa·m$^{1/2}$]	1.2	1.1	1.0	0.75	0.75	0.75
t_{in} [h]	4.2 ± 0.8	12	16.9	- [1]	- [1]	- [1]
t_f [h]	37.2 ± 5.3	43.5 ± 1	41.6	18.9 ± 2.4	20.3 ± 2.6	1 ± 0.5

1) Could not be determined due to the coarse resolution of the crosshead displacement signal
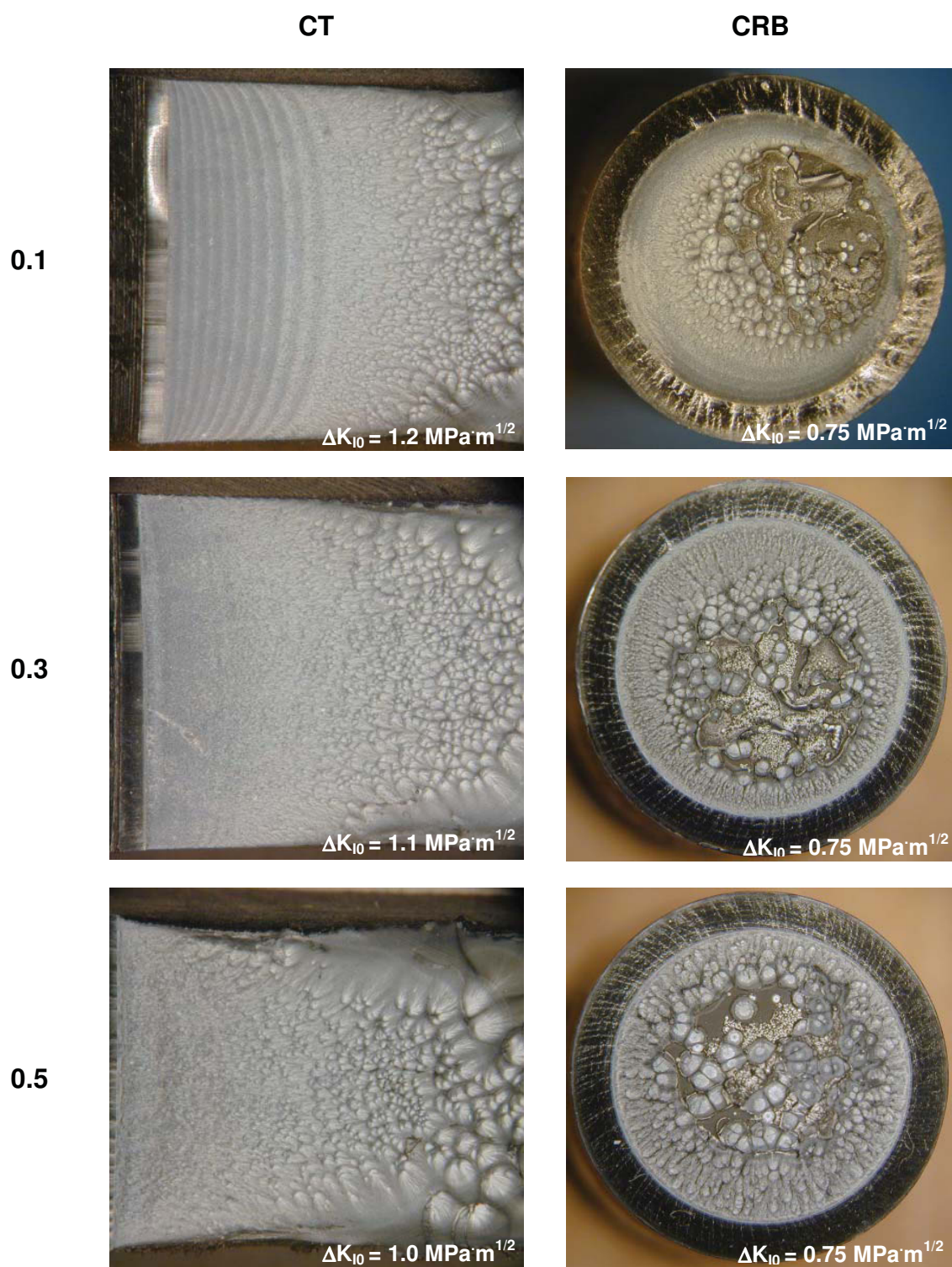
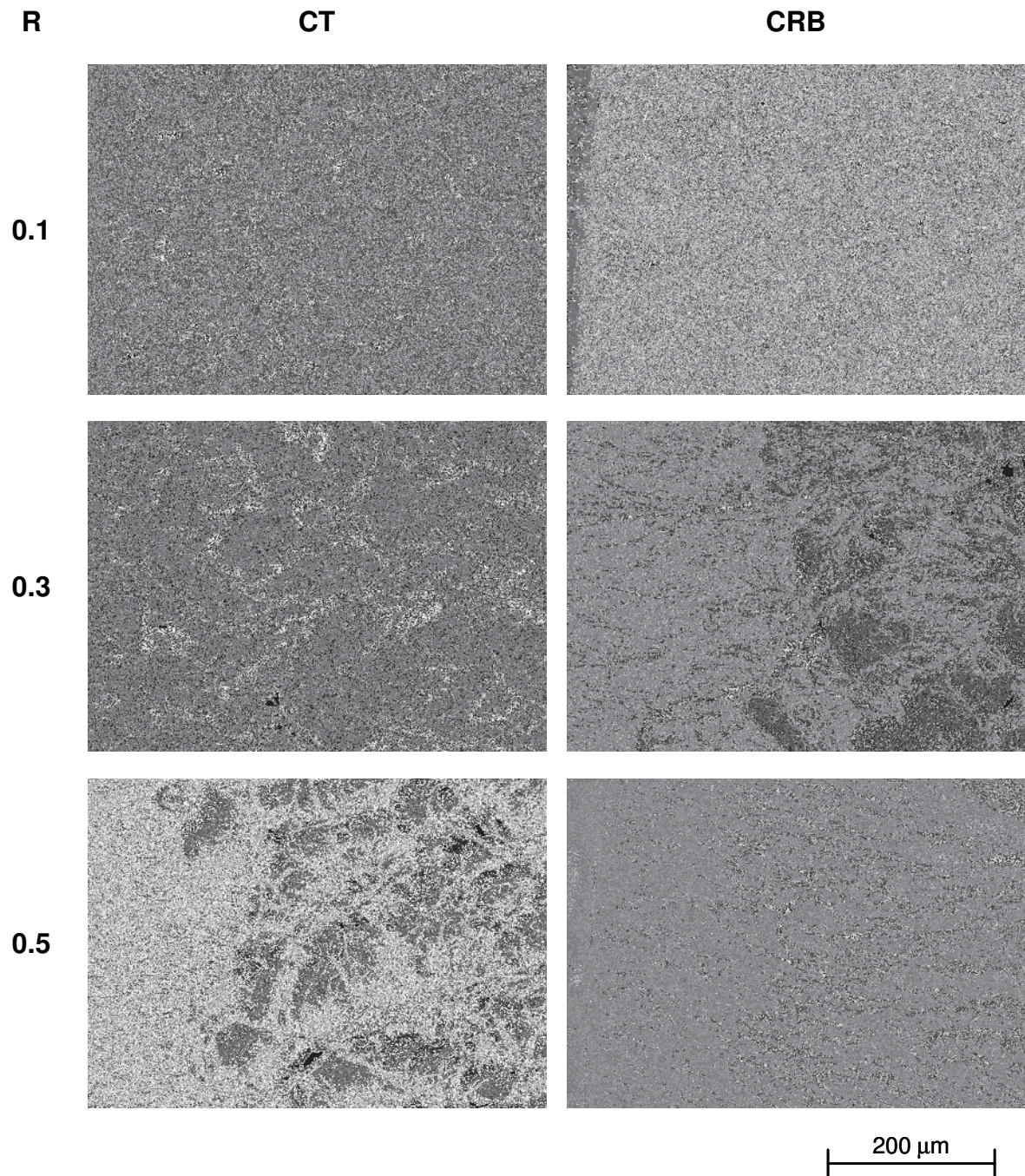**Fig. 4.18:** Optical photos of PE100-1 after testing at various R-ratios (23 ℃, 5 Hz).

Fig. 4.19: SEM photos of PE100-1 in the region of crack initiation (magnification factor of 200) after testing at various R-ratios (23 °C, 5 Hz).

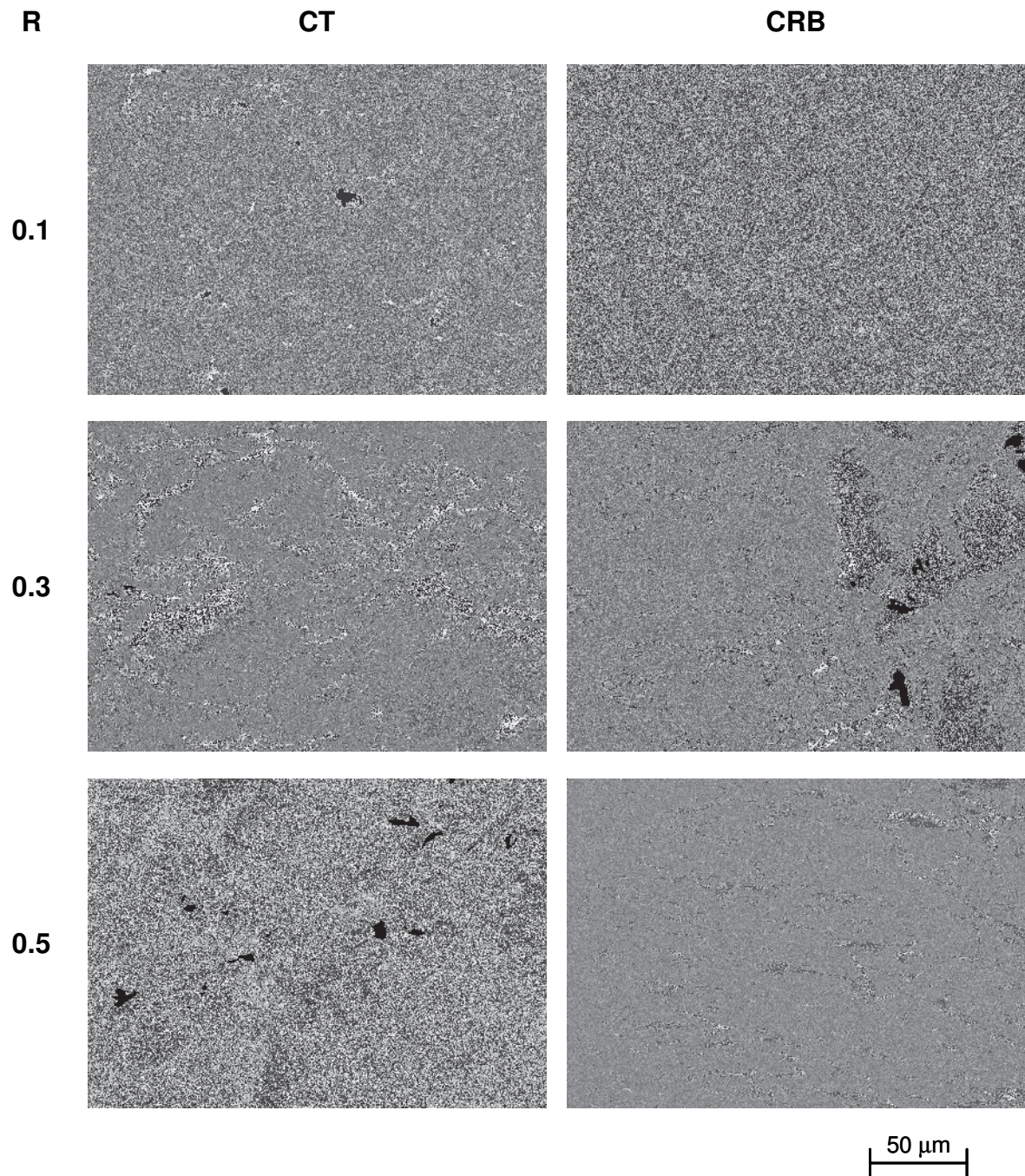**Fig. 4.20:** SEM photos of PE100-1 in the region of crack initiation (magnification factor of 500) after testing at various R-ratios (23 °C, 5 Hz).
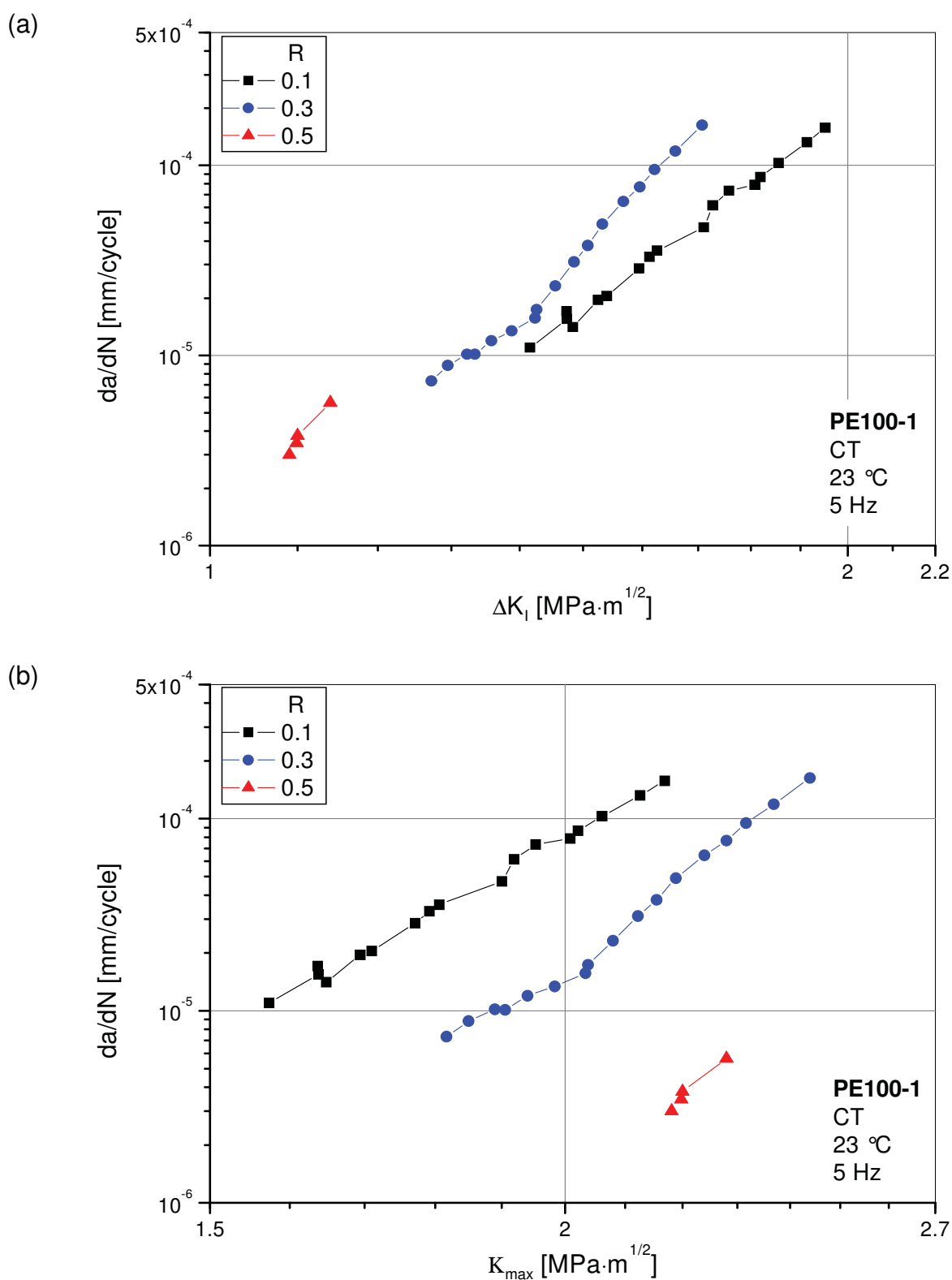
(a)

(b)

Fig. 4.21: FCG rates in PE100-1 as a function of (a) ΔK_I and (b) K_{Imax} (23 °C, 5 Hz), using CT specimens and various R-ratios.

5   Summary and Conclusions

Fatigue crack growth (FCG) experiments were conducted on three different high density polyethylene (PE-HD) pipe grades using two test specimen configurations (compact type, cracked round bar) under a sinusoidal load at frequencies of 5, 10 and 30 Hz, R-ratios (F_{min}/F_{max}) of 0.1, 0.3 and 0.5 and a test temperature of 23 °C.

A discontinuous crack growth mechanism was characteristic for all materials investigated using CT specimens. It was found that the FCG resistance of PE100-3 was clearly the highest among the three selected polyethylenes, while the highest FCG rates were observed in PE100-1 (a black carbon-filled type). Based on the available information on molecular and morphological parameters, the molecular weight was assumed to be the most influential parameter for the increased FCG resistance of PE100-3. The crack growth inside the specimen was higher than on the outside, which can be seen in the semi-elliptical shape of the front-line of the crack. Generally, the fracture surfaces reveal the remnants of voids and fibrils, typical attributes of craze formation and breakdown. The arrest lines that are typical for discontinuous crack growth are quite similar in all investigated materials and the fracture surfaces are characterized by an enhanced micro-ductility.

In order to check the influence of different specimen types on FCG results, tests were also conducted using CRB specimens. Quasi-brittle cracks could be initiated, but it was very difficult to achieve symmetrically growing cracks. Comparing the results obtained with CT and CRB specimens, appropriate correlations could be observed. On the basis of the results gained so far, testing time was clearly reduced by using CRB instead of CT specimens, which could be of particular interest when ranking of materials is the goal. The fracture surface of CRB specimens showed similar structures to those found in CT specimens, like voids and fibrils, but the prominent striations on the fracture surfaces seen in CT specimens were not so clearly pronounced in CRB specimens.

The effects of frequency may be considered significant in the low crack growth region. When examining the FCG data it becomes apparent that with increasing test frequency there was a noticeable increase in crack growth resistance in CT

specimens in the low crack-growth regime, while in CRB specimens no differences could be found because of the large scatter band. For all investigated frequencies, a temperature increase resulting from hysteretic heating was measured at the crack tip in CT specimens. The strongest effects were measured at 30 Hz, where crack-tip heating was distinctly increased.

In terms of ΔK_I the fatigue crack growth rates were found to strongly depend on the R-ratio. In the case of $R = 0.5$ (testing with CT specimens), the validity of LEFM was limited to low da/dN-values and low ΔK_I-values. Since a shift of the curve to the left was observed with increasing R-ratio, FCG rates in PE100-1 are not only controlled by the stress intensity factor range at the defined test parameters, but also by the maximum stress intensity factor and/or the mean stress intensity factor. There may be a tendency for higher crack growth rates at higher R-ratios as a result of more creep crack extension associated with the higher maximum and mean stress intensity levels.

6 Literature

Bäckman, M., and Lind, C. (2001).

Balika, W., Pinter, G., Choi, B.-H., and Lang, R. W. (2004). In Proc. "Antec 2004", 4028-4032, Chicago (USA), May 16-20.

Beech, S. H., and Clutton, E. Q. (2004).

Beech, S. H., Palmer, S. J., and Burbidge, R. W. (1997). In Proc. "International Plastic Pipe Symposium", 205-214.

Beer, G., Vogt, M., Wiesecke, J., and Auffernamm, J. (2005). Kunststoffe 10, 46.

Brown, N., and Lu, X. (1994). ASTM STP 1223, 234.

Brown, N., and Lu, X. (1995). Polym. 36, 543.

Bucknall, C. B., and Dumpleton, P. (1985). Plast. Rubb. Proc. Appl. 5, 343.

Chudnovsky, A. (1984). "Crack Layer Theory" N174634, NASA Report.

Chudnovsky, A., Shulkin, Y., Baron, D., and Lin, K. P. (1995). J. Appl. Polym. Sci. 56, 1465.

Clark, T. R., Hertzberg, R. W., and Manson, J. A. (1990). J. Test. Eval. 18, 319.

DesLauriers, P. J., McDaniel, M. P., Rohlfing, D. C., Krishnaswamy, R. K., S.J., S., Maeger, P. L., Benham, E. A., A.R., W., Sukhadia, A. M., and Beaulieu, W. M. (2005). In Proc. "ANTEC 2005", Chicago, US.

Domininghaus, H. (1997). "Die Kunststoffe und ihre Eigenschaften", Springer Verlag, Berlin.

Dörner, G., and Lang, R. W. (1997). 3R international 36, 672.

Dragaun, H., and Kratochvilla, T. (2004). In Proc. "18. Leobener Kunststoff-kolloquium", Leoben.

Egan, B. J., and Delatycki, O. (1995). J. Mater. Sci. 30, 3307.

Ertl, J., Luderer, J., and Mieden, O. (2004). Kunststoffe 10, 53.

Fanesi, E. (2003). "Characterization of crack growth in high density polyethylene under static and cyclic loading", Diploma thesis, Dipartimento di Chimica, Politecnico di Milano, I.

Favier, V., Giroud, T., Strijko, E., Hiver, J. M., G´Sell, C., Hellinckx, S., and Gold-berg, A. (2002). Polym. 43, 1375.

Fleissner, M. (1987). Kunststoffe 77, 45.

Fleissner, M. (1998). Polym. Eng. Sci. 38, 330.

Fuchs, F. (2006). "Through-thickness process zone characterization at fatigue cracks in PE-HD", Diploma thesis, Institute for Material Science and Testing of Plastics

of the University of Leoben, Montanuniversität, Leoben.

Glenz, W. (2004). Kunststoffe 10, 58.

Grosse-Boes, R., and Kloth, R. (2004). 3R international 43, 233.

Ha, C.-S., Kim, Y., Lee, W.-K., Cho, W.-J., and Kim, Y. (1998). Polym. 39, 4765.

Haager, M., Pinter, G., and Lang, R. W. (2004). In Proc. "ANTEC", 4023-4027, Chicago.

Haager, M., Pinter, G., and Lang, R. W. (2006). In Proc. "ANTEC" (S. o. P. Engineers, Ed., Charlotte, North Carolina.

Haager, M., Zhou, W., Pinter, G., and Chudnovsky, A. (2005a). In Proc. "Antec 2005", 3538-3542, Boston (USA), May 1-5.

Haager, M., Pinter, G., Balika, W., and Lang, R. W. (2005b). In, Merseburg.

Hertzberg, R. W., and Manson, J. A. (1980). Academic Press, New York.

Hertzberg, R. W., and Manson, J. A. (1989). In "Deformation and fracture mechanics of engineering materials" (A. Press, Ed.), John Wiley & Sons, New York.

Hessel, J. (2001). 3R international 40, 178.

Hessel, J., and Maurer, E. (1994). Materialprüfung 6.

Hiesch, T. (2005). "Charakterisierung des spröden Risswachstums in Polyethlyen-Rohrwerkstoffen mit beschleunigten Prüfmethoden", Diplomarbeit, Institut für Werkstoffkunde und Prüfung der Kunststoffe, Montanuniversität, Leoben.

Hiesch, T., Haager, M., Pinter, G., and Lang, R. W. (2005). In Proc. Merseburg.

Hohenadel, R., rehm, T., and Mieden, O. (2005). Kunststoffe 10, 38.

Hu, Y., Summers, J., Hiltner, A., and Baer, E., J (2003). Mat. Sci. 38, 633.

Hubert, L., David, L., Séguéla, R., Vigier, G., Degoulet, C., and Germain, Y. (2001). Polym. 42, 8425.

Janson, L. E. (1999). "Plastic Pipes for Water Supply and Sewage Disposal", Borealis, Stockholm.

Kadota, K., Chum, S., and Chudnovsky, A. (1993). J. Appl. Polym. Sci. 49, 863.

Karger-Kocsis, J. (1995). In "Polypropylene - Structure, blends and composites" (J. Karger-Kocsis, Ed.), Vol. 3: Composites, 142-201, Chapman & Hall, London (UK).

Kasakevich, M. L., Moet, A., and Chudnovsky, A. (1990). Polymer 31, 435.

Kausch, H.-H. (1986). In "Failure of Plastics" (W. Brostow and R. D. Corneliussen, Eds.), 84-97, Hanser, Munich.

Kim, H. S., and Wang, X. M. (1994). J. Mater. Sci. 29, 3209.

Kissin, Y. V. (1996). "Encyclopedia of chemical technology", John Wiley & Sons, New York.

Kramer, E. J., and Berger, L. L. (1990). In "Advances in Polymer Science" (H.-H. Kausch, Ed.), 2, 1-68, Springer, Berlin Heidelberg.

Kratochvilla, T., Muschik, H., and Dragaun, H. (2005). Kunststoffe 6, 53.

Krumme, A., Lehtinen, A., and Viikna, A. (2003). European Polymer Journal 40, 359.

Kuske, H.-D., and Bastian, M. (2004). 3R international 43, 497.

Lang, R. W. (1984). "Applicability of Linear Elastic Fracture Mechanics to Fracture in Polymers and Short-Fiber Composites", Ph.D. Dissertation, Lehigh University, Bethlehem, Pennsylvania.

Lang, R. W. (1997). 3R international 36, 40.

Lang, R. W., Stern, A., and Dörner, G. (1997). Angew. Makromol. Chem. 247, 131.

Lang, R. W., Balika, W., and Pinter, G. (2004). In "The application of fracture mechanics to polymers, adhesives and composites" (D. R. Moore, Ed.), ESIS publication 33, 83-92, Elsevier, Oxford (UK).

Lang, R. W., Pilz, G., Pinter, G., and Stern, A. (2000). Plastics Special 6, 26.

Laurent, E. (2001). In Proc. "Plastic Pipes XI", 63-73, München, D.

Lawrence, C., Teo, S., and Potter, R. (1998). In Proc. "Plastic Pipes X", 743, Göteborg (S).

Lederer, K., and Forster, E. (1984). In "Polymere Werkstoffe", 3, Kapitel 1, Georg Thieme Verlag, Stuttgart.

Li, L., and Wang, Q. (2003). Journal of Polymer Science, Part A: Polymer Chemistry 42, 5662.

Miannay, D. P. (2001). "Time-Dependent Fracture Mechanics", Springer, New York.

Nezbedova, E., Kucera, J., and Zahradnickova, A. (2001). Mech. Time-Dep. Mater. 5, 67.

Nishimura, H., Nakashiba, A., and Nakakura, M. (1993). Polym. Eng. Sci. 33, 895.

Parsons, M., Stepanov, E. V., Hiltner, A., and Baer, E. (1999). J. Mater. Sci. 34, 3315.

Parsons, M., Stepanov, E. V., Hiltner, A., and Baer, E. (2000a). J. Mater. Sci. 35, 2659.

Parsons, M., Stepanov, E. V., Hiltner, A., and Baer, E. (2000b). J. Mater. Sci. 35, 1857.

Parsons, M., Stepanov, E. V., Hiltner, A., and Baer, E. (2001). J. Mater. Sci. 36, 5747.

Pinter, G. (1999). "Crack growth behavior of PE-HD under static loading conditions", Ph.D. Thesis, Institute of Materials Science and Plastics Testing, University of Leoben, Leoben.

Pinter, G., and Lang, R. W. (2003). J. Appl. Polym. Sci. 90, 3197.

Pinter, G., and Lang, R. W. (2004). In "The application of fracture mechanics to polymers, adhesives and composites" (D. R. Moore, Ed.), ESIS publication 33, 47-54, Elsevier, Oxford (UK).

Pinter, G., Balika, W., and Lang, R. W. (2000). In Proc. "ECF 13, 13th European Conference on Fracture", San Sebastian (E), September 06-09.

Pinter, G., Balika, W., and Lang, R. W. (2002a). In "Temperature-Fatigue Interaction" (L. Remy and J. Petit, Eds.), 29, 267-275, Esis Publication, Amsterdam.

Pinter, G., Balika, W., and Lang, R. W. (2002b). In.

Pinter, G., Balika, W., and Lang, R. W. (2002c). In "Temperature Fatigue Interaction" (L. Rémy and J. Petit, Eds.), ESIS publication 29, 267-275, Elsevier, Amsterdam.

Plummer, C. J. G., Goldberg, A., and Ghanem, A. (2001). Polym. 42, 9551.

Plummer, C. J. G., Goldberg, A., and Ghanem, A. (2003). In "Fracture of Polymers, Composites and Adhesives II" (B. R. K. Blackman, A. Pavan and J. G. Williams, Eds.), 3-14, Elsevier Ltd. and ESIS.

Ramsteiner, F. (2004). In "The application of fracture mechanics to polymers, adhesives and composites" (D. R. Moore, Ed.), ESIS publication 33, 31-37, Elsevier, Oxford (UK).

Reynolds, P. T., and Lawrence, C. C. (1991). J. Mater. Sci. 26, 6197.

Reynolds, P. T., and Lawrence, C. C. (1993). J. Mater. Sci. 28, 2277.

Rimnac, C. M. (1983). "The fatigue crack propagation response and fracture surface micromorphology of neat and rubber- modified poly(vinyl chloride)", Lehigh University, USA.

Saxena, A. (1998). "Nonlinear Fracture Mechanics for Engineers", CRC Press LLC, Boca Raton.

Scholten, F. L., Pisters, J., and Venema, B. (1998). Polymer Testing 17, 385.

Scholten, F. L., Gueugnat, D., and Berthier, F. (2001). In Proc. "Plastic Pipes XI", 1115-1126, Munich.

Shah, A., Stepanov, E. V., Klein, M., Hiltner, A., and Baer, E. (1998a). Int. J. Fract. 84, 159.

Shah, A., Stepanov, E. V., Klein, M., Hiltner, A., and Baer, E. (1998b). J. Mater. Sci. 33, 3313.

Shah, A., Stepanov, E. V., Capaccio, G., Hiltner, A., and Baer, E. (1998c). J. Polym. Sci. Part B: Polym. Phys. 36, 2355.

Skibo, M. D. (1977). "The effect of frequency, temperature and materials structure on fatigue crack propagation in polymers", Lehigh University, USA.

Soares, J. B. P., and Kim, J. D. (1999). Journal of Polymer Science, Part A: Polymer Chemistry 38, 1408.

Song, M. M., Hu, G. X., and Hu, L. J. (1998). Polym. Test. 17, 311.

Stern, A. (1995). "Fracture mechanical characterization of the long-time behavior of polymers under static loads", Ph.D. Thesis, Institute of Materials Science and Plastics Testing, University of Leoben, Leoben (A).

Strebel, J. J., and Moet, A. (1995). J. Polym. Sci. Part B: Polym. Phys. 33, 1969.

van der Grinten, F., and Wichers Schreur, P. W. M. (1996). Plast. Rubb. Compos. Proc. Appl. 25, 294.

Williams, J. G. (1987). In "Fracture Mechanics of Polymers" (E. H. Limited, Ed.), Chichester.

Yngvesson, M. (2000). Int. J. Fract. 102, L9.

Zhou, Y.-Q., and Brown, N. (1989). J. Mater. Sci. 24, 1458.

Zhou, Y.-Q., and Brown, N. (1992). J. Polym. Sci. Part B: Polym. Phys. 30, 477.